T.R.

GEBZE TECHNICAL UNIVERSITY

GRADUATE SCHOOL OF NATURAL AND APPLIED SCIENCES

FABRICATION AND CHARACTERIZATION OF BISMUTH OXIDE-BASED BILAYER ELECTROLYTES FOR SOLID OXIDE FUEL CELLS

BATUHAN BAL

A THESIS SUBMITTED FOR DEGREE OF

MASTER OF SCIENCE

DEPARTMENT OF MATERIALS SCIENCE AND ENGINEERING

GEBZE

2021

T.R.

GEBZE TECHNICAL UNIVERSITY

GRADUATE SCHOOL OF NATURAL AND APPLIED SCIENCES

FABRICATION AND CHARACTERIZATION OF BISMUTH OXIDE-BASED BILAYER ELECTROLYTES FOR SOLID OXIDE FUEL CELLS

BATUHAN BAL

A THESIS SUBMITTED FOR DEGREE OF

MASTER OF SCIENCE

DEPARTMENT OF MATERIALS SCIENCE AND ENGINEERING

THESIS SUPERVISOR

ASSIST. PROF. DR. ALIGUL BUYUKAKSOY

GEBZE

2021

T.C.
GEBZE TEKNİK ÜNİVERSİTESİ
FEN BİLİMLERİ ENSTİTÜSÜ

KATI OKSİT YAKIT HÜCRELERİ İÇİN BİZMUT OKSİT TEMELLİ ÇİFT KATMANLI ELEKTROLİTLERİN ÜRETİMİ VE KARAKTERİZASYONU

BATUHAN BAL

YÜKSEK LİSANS TEZİ
MALZEME BİLİMİ VE MÜHENDİSLİĞİ ANABİLİM DALI

DANIŞMANI
DR. ÖĞR. ÜYESİ ALİGÜL BÜYÜKAKSOY

GEBZE
2021

GEBZE TEKNİK ÜNİVERSİTESİ	**YÜKSEK LİSANS JÜRİ ONAY FORMU**

GTÜ Fen Bilimleri Enstitüsü Yönetim Kurulu'nun 08/01/2021 tarih ve 2021/02 sayılı kararıyla oluşturulan jüri tarafından 14/01/2021 tarihinde tez savunma sınavı yapılan Batuhan Bal'ın tez çalışması Malzeme Bilimi ve Mühendisliği Anabilim Dalında YÜKSEK LİSANS tezi olarak kabul edilmiştir.

JÜRİ

ÜYE
(TEZ DANIŞMANI) : Dr. Öğretim Üyesi Aligül Büyükaksoy

ÜYE : Dr. Öğretim Üyesi Begüm Ünveroğlu

ÜYE : Prof. Dr. Ahmet Yavuz Oral

ONAY

Gebze Teknik Üniversitesi Fen Bilimleri Enstitüsü Yönetim Kurulu'nun

..…/……/…… tarih ve ……/…..... sayılı kararı.

SUMMARY

Solid oxide fuel cells (SOFCs) have not been commercialized yet due to high operating temperatures that cause chemical and microstructural degradation, which result in performance losses upon long-term operation. Therefore, lowering the operating temperature below 650 °C is a promising approach. However, this approach leads to slow reaction kinetics.

Bismuth oxide-based electrolytes are promising candidates for SOFCs because of their immense ionic conductivity. However, bismuth oxide-based materials reduce to metallic Bi when it is exposed to hydrogen at the targeted SOFC operating temperatures. In this thesis, we aimed to prevent the reduction of bismuth oxide by depositing a thin, chemically stable ionic conductor film onto the fuel side of the bismuth oxide-based ceramic.

A thin yttria-stabilized zirconia (YSZ) layer was deposited onto YDB ceramic using a cost-effective and facile polymeric precursor method. The optimum deposition parameters of YSZ thin films were investigated. The generic YSZ polymeric precursor i) reacts with the YDB substrate to form bismuth yttrium oxychloride and ii) leads to crack formation due to unpolymerized reactants in the deposited thin film. Switching from the generic YSZ polymeric precursor to a newly developed one, which consists of zirconium oxynitrate instead of zirconium oxychloride, suppressed crack formation in deposited thin films.

Crack formation in thin films, possible reactions between the substrate and thin films were investigated by scanning electron microscopy (SEM), x ray diffraction (XRD) and energy dispersive spectroscopy (EDX), respectively. Electrical conductivities and blockage properties of developed YSZ films were investigated by electrochemical impedance spectroscopy and open-circuit voltage measurements, respectively.

Keywords: Solid Oxide Fuel Cell, Bi-layer Electrolytes, Bismuth Oxide, YSZ thin films, Open Circuit Voltage.

ÖZET

Katı oksit yakıt hücreleri (KOYH) yüksek çalışma sıcaklarından dolayı oluşan kimyasal ve mikroyapısal bozunmaların sebep olduğu performans kayıpları sebebiyle henüz ticari bir ürün haline gelememiştir. Bu performans kayıplarının üstesinden gelmek için, çalışma sıcaklıklarının 650 °C altına düşürülmesi gelecek vaadeden bir yaklaşımdır. Ancak, çalışma sıcaklıklarını düşürmek yavaş reaksiyon kinetiğine sebebiyet verir.

Bizmut oksit bazlı elektrolitler, yüksek iyonik iletkenliklerinden dolayı KOYH'lar için iyi birer adaydır. Ancak, saf bizmut oksit; hedeflenen KOYH şartlarında metalik Bi'a indirgenmektedir. Bu tezde, koruyucu ve iyonik iletken bir katman kullanarak bizmut oksitin indirgeyici ortamlarda indirgenmesini önlemek hedeflenmiştir.

Itriya stabilize zirkonya (YSZ) katman, etkili ve ekonomik polimerik öncü çözelti yöntemi kullanılarak YDB seramiklerin üzerinde biriktirilmiştir. YSZ filmlerin optimum biriktirme şartları araştırılmıştır ve geleneksel YSZ polimerik öncüsü kullandığında, öncünün ii) altlıkla reaksiyona girip bizmut itriyum oksiklorit oluşturduğu ve i) polimerleşmesi tamamlanmadığından dolayı çatlak oluşumuna sebep verdiği gözlenmiştir. Geleneksel YSZ polimerik öncüsü, yeni geliştirilmiş olan ve zirkonyum oksiklorit yerine zirkonyum oksinitrat bulunduran YSZ polimerik öncüsüyle değiştirildiğinde biriktirilen ince filmlerdeki çatlak oluşumu önlenmiştir.

Filmlerdeki çatlak oluşumu taramalı elektron mikroskobuyla (SEM), altlık ve ince filmler arasında gerçekleşebilecek reaksiyonlar ise x ışını kırınımı ve enerji dağılımlı x ışını spektroskopisi ile incelenmiştir. İnce filmlerin iletkenliği elektrokimyasal empadans spektroskopisi ve bloklayıcı özelliği açık devre potansiyeli ölçümleriyle incelenmiştir.

Anahtar kelimeler: Katı Oksit Yakıt Hücresi, Çift Katmanlı Elektrolitler, Bizmut Oksit, YSZ ince filmler, Açık Devre Potansiyeli.

ACKNOWLEDGEMENTS

I am very grateful for his support during my thesis to my supervisor, Dr Aligül Büyükaksoy, who continues to enlarge my horizon even after my thesis work and inspires me through his experiences and lifestyle.

I am also really grateful to Dr. Kerem Özgür Gündüz who always shares his experience on similar topics when I am struggling with some ideas about my thesis.

And also, I would like to express my sincere and thanks to my all colleagues for their supports.

I am thankful that the project (217M031) is funded by The Scientific and Technological Research Council of Turkey (TUBITAK).

TABLE OF CONTENTS

LIST OF ABBREVIATIONS AND ACRONYMS

Abbreviations and Acronyms		**Explanations**
$\sigma_{electronic}$	:	Ionic Conductivity
σ_{ionic}	:	Electronic Conductivity
t_{O2-}	:	Oxygen Transfer Number
ASR	:	Area Specific Resistance
CHP	:	Combine Heat and Power
E	:	Potential
E^0	:	Standart Potential
EDX	:	Energy Dispersive X-Ray Analysis
EIS	:	Electrochemical Impedance Spectroscopy
ESB	:	Erbia Stabilized Bismuth Oxide
F	:	Faraday Constant
GDC	:	Gadolinia Doped Ceria
I	:	Current
IT-SOFC	:	Intermadiate Temperature Solid Oxide Fuel Cell
LSC	:	Lanthanum Strontium Cobalt
LSM	:	Lanthanum Strontium Manganese
MIEC	:	Mixed Ionic-Electronic Conductor
n	:	Electron Number
OCV	:	Open Circuit Voltage
ORR	:	Oxygen Reduction Reaction
PEG	:	Polyethylene Glycol
PEM	:	Polymer Electrolyte Membrane
R	:	Ideal Gas Constant
S	:	Siemens
SEM	:	Scanning Electron Microscopy
SOFC	:	Solid Oxide Fuel Cell

TPB	:	Triple Phase Boundary
TM	:	Transition Metals
XRD	:	X-ray Diffraction
YDB	:	Yttria Doped Bismuth Oxide
YSZ	:	Yttria Stabilized Zirconia

LIST OF FIGURES

LIST of TABLES

1. INTRODUCTION

1.1. The Energy Problem

Creating a sustainable energy system on a global scale is a challenging issue while the human population is growing faster today. The use of conventional fuel sources, such as coal, oil, and gas cause harmful gas emission that strongly affect climate change around the world. According to the International Energy Agency, an immense rising in carbon dioxide emission would be observed from 32 Gt $year^{-1}$ in 2013 to 44 Gt $year^{-1}$ in 2040 with an increase in industrialization [1]. The increase of CO_2 emission causes climate change by trapping heat on the surface of the earth. That effect occurs because the greenhouse gases released into the atmosphere keep excessive heat in the atmosphere and is called the greenhouse effect. Fossil fuels and non-renewable energy sources have caused, not just harm to the environment, but also a deficit in underground sources. Therefore, the crucial importance of renewable energy is that overcoming well-established climate change problems and increment the efficiency of energy production [2].Renewable energy sources, such as; wind and solar energy could pave the way to overcoming the crucial energy problems of the world. However, these new approaches suffer from intermittency of energy production, which renders the development of complimentary energy conservation and storage technologies extremely important [2]. Devices that enable storage of energy during high production times (i.e., when it is windy or during day time for wind and solar energies, respectively) and those that can convert stored energy into electricity during low production times (i.e., when the weather is still or during night time for wind and solar energies, respectively) can ensure the effectiveness of the renewable energy technologies. Fuel cells are promising candidates for such purposes, due to their ability for continuous energy production and high efficiency between 40% and 60% [3].

Fuel cells are basically devices which can convert chemical energy into electricity via electrochemical oxidation of fuel (hydrogen in most cases) and reduction of oxygen.

There are a number of different types of fuel cells, most of which are defined by the ionic conductor electrolyte material they use. One of the most intensely studied fuel cells types, PEM fuel cells can be operated at temperatures as low as ca. 80 °C, owing to their fast proton conductor Nafion electrolyte and the extremely active electrodes decorated with Pt nanoparticles [4]. The high cost of this type of fuel cells dictated by the use of Pt is the main challenge that needs to be overcome in for the widespread commercial use of these devices [4].

Another major type of fuel cell is the solid oxide fuel cells (SOFCs), ceramic oxygen ion conductor electrolyte-based systems, which, when used in a combined heat and power (CHP) scenario, can provide up to 90% efficiency [5]. The high operating temperatures of 700-900 °C provides ability to operate using a wide range of fuels, including hydrocarbons, but, render these systems quite prone to long-term performance degradation by inducing microstructural and chemical deterioration. As a result, lowering the operating temperatures of SOFCs down to ca. 600 °C has been widely studied [5]. This task is extremely challenging, mainly because lowering operating temperatures causes extremely retarded electrochemical reaction and ionic transport kinetics. In this thesis, an electrolyte-supported solid oxide fuel cell design, which can enable low-temperature fabrication of electrode layers and thereby achievement of high performance even at 600 °C is envisioned. To achieve low electrolyte resistances even at these low temperatures, the utilization of the extremely fast ion conductor yttria doped bismuth oxide is presented. Methods, such as application of protective coatings, are explored to ensure chemical and structural stability of these electrolytes under SOFC conditions.

2. FUEL CELLS

2.1. Introduction to Fuel Cells

Fuel cells effectively produce electricity by converting chemical energy into electrical energy through electrochemical reactions. Fuel cells were proposed as an alternative to voltaic batteries by Charles Langer and Ludwig Mond in 1889 [6]. They discovered a porous, solid electrolyte instead of sulfuric acid-containing aqueous solution as an electrolyte that led to more stable currents [6].

2.2. General Working Principles of Solid Oxide Fuel Cells

A solid oxide fuel cell consists of two porous electrodes (the anode and cathode) which are separated by a dense, leakage-free and, ion conductive electrolyte membrane (Fig 2.1). Fuel, especially hydrogen, is fed to the fuel side where the oxidation of hydrogen occurs, and the electrons are released to the outer circuit. On the other side, oxidant, in most cases is oxygen, is fed to the air side where the reduction of oxygen occurs, and the electrons are accepted by the outer circuit. The electron flow through the outer circuit causes an electrical current. The fuel fed causes a chemical potential between the air and fuel side, and that chemical potential causes an electrical potential through the external circuit. The relationship between chemical and an electrical potential is expressed with Nernst equation is given below:

$$E = E^{o} + \frac{R.T}{n.F}\ln\left(\frac{p_{H_2O}}{p_{H_2}p_{O_2}^{1/2}}\right) \quad (2.1)$$

where the E^0 is the standard cell potential, R is the ideal gas constant, T is the temperature, n is the electron number, and F is the Faraday constant and equals to

$9.65x10^4$ C/mol. According to the Nernst equation, the partial pressure of the reactants and the products determine that the open circuit potential.

The general working principle is similar among fuel cells and pervasive reactions take place in the system that strongly depends upon fuel type. In the situation of the use of hydrogen as a fuel, the reactions would occur that is given below:

$$H_2 + O^{-2} \rightarrow H_2O + 2e^- \quad (2.2)$$

$$O_2 + 4e^- \rightarrow 2O^{-2} \quad (2.3)$$

Reaction 2.2 takes place at the anode and reaction 2.3 takes place at the cathode.

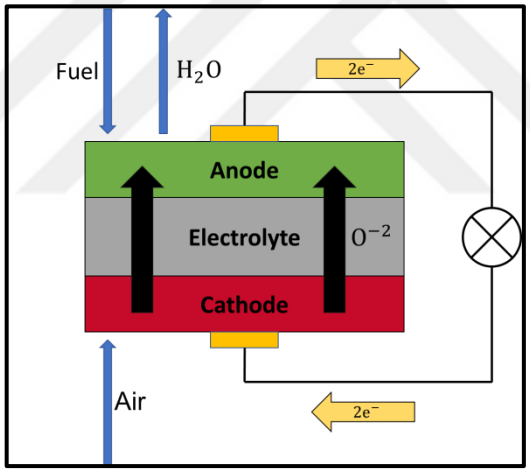

Figure 2. 1: General Working Principle of SOFCs.

2.3. Components of Solid Oxide Fuel Cells

2.3.1. Cathode

Air electrodes (cathodes) are operated at extremely oxidizing environments to ensure oxygen reduction. Cathode materials for SOFCs must have high electrocatalytic activity for oxygen reduction and electronic conductivity at operating conditions. Perovskite structured (La, Sr)TMO_3, where TM is one of the transition metals Mn, Fe or

Co, meets the electrocatalyst material requirements and thus, are used widely [6, 7]. For efficient delivery of the generated oxygen ions, the electrocatalyst material is mixed with an ionic conductor (usually the same material as that used for the electrolyte). In this composite cathode layer, maximum electrode performance can be ensured by maximizing the electrocatalyst-ionic conductor-gas (pore) triple phase boundary (TPB) length, where the oxygen reduction takes place effectively. Long TPBs correspond to a fine microstructure, which can be achieved by low-temperature processing methods.

2.3.2. Anode

Fuel electrodes (anodes) require high electrocatalytic activity and electronic conductivity under fuel flow and at operating temperatures for effective SOFC operation. In a similar way to cathodes, it also common practice for the electrocatalyst (usually metallic Ni) to be mixed with an ionic conductor – typically the electrolyte material – to achieve long TPB length and thus, enhanced electrochemical reaction sites.

Under the fuel flow, the oxygen partial pressure would be extremely low (ca. 10^{-16} atm), which ensures that Ni remains in its metallic state. However, it is expected that up to ten interruptions in the fuel supply are expected in the lifetime of a fuel cell [8]. This, in turn, causes the anode compartment atmosphere to become oxidizing and induces a Ni to NiO conversion. One of the major issues of the SOFC anodes is the mechanical failure of the anode due to the stresses associated with the volume expansion accompanying the Ni oxidation [8].

2.3.3. Electrolyte

In contrast to electrodes, electrolytes must have dense and leakage-free microstructures to be able to prevent mixing of fuel and oxidant gases that are fed to the anode and cathode sides of SOFCs. Mixing of these gases causes minimized chemical potential gradient and consequently, minimization of the cell power output. It is crucial that the electrolyte material is an oxygen ion conductor, but an electron insulator. The ratio of ionic conductivity (σ_{ionic}) to the total electrical conductivity ($\sigma_{ionic} + \sigma_{electronic}$) is

defined as the oxygen transfer number (t_{O2-}), which is preferably equal to unity for the electrolyte material under both reducing and oxidizing conditions.

Since the ionic transport through the electrolyte lattice is a thermally activated diffusion process, lowering the operating temperatures lower the ionic conductivity. It is therefore crucial that, to reduce the ohmic electrolyte resistances, the electrolyte material is produced as thin as possible.

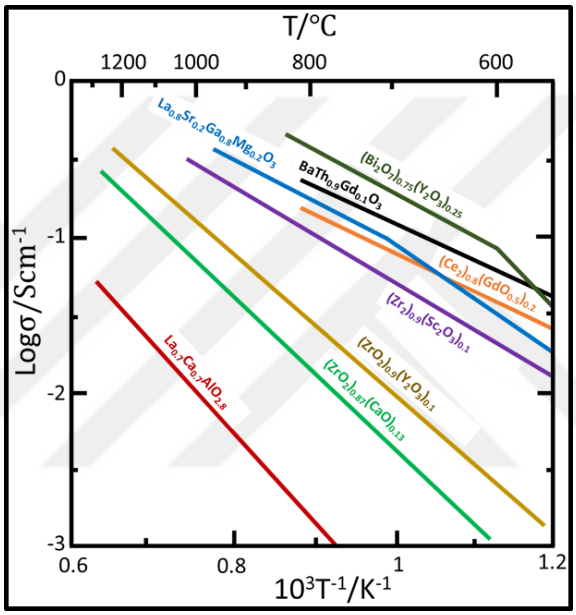

Figure 2. 2: Temperature dependence of ionic conductivity for various electrolyte materials.

Figure 2.2 provides a comparison of temperature dependencies of electrical conductivities of potential SOFC electrolyte materials. Among them, Yttria-stabilized zirconia (YSZ) with the cubic fluorite structure is the most widely used electrolyte material, despite the fact that it is not the fastest ion conductor. However, YSZ has an oxygen transfer number equal to unity, it is chemically compatible with other cell components, and it is structurally and chemically stable under air or fuel flow conditions, at high temperatures. The fluorite structure is a face centered cubic system according to cation placement and anions are located at all tetrahedral sites (Figure 2.3). This arrangement causes a high amount of octahedral interstitial vacancies. Electrolytes have a mechanism about transferring oxygen vacancies through whole electrolyte body.

To be able to provide that mechanism, electrolyte structure must have oxygen vacancies. The oxygen vacancies are created by additional dopants that have lower valance value than Zr cations. Additional dopant reactions are declared in Kröger – Vink notation, as follows:

$$Y_2O_3 \xrightarrow{ZrO_2} 2Y'_{Zr} + 3O_O^x + V_{\ddot{O}} \tag{2.4}$$

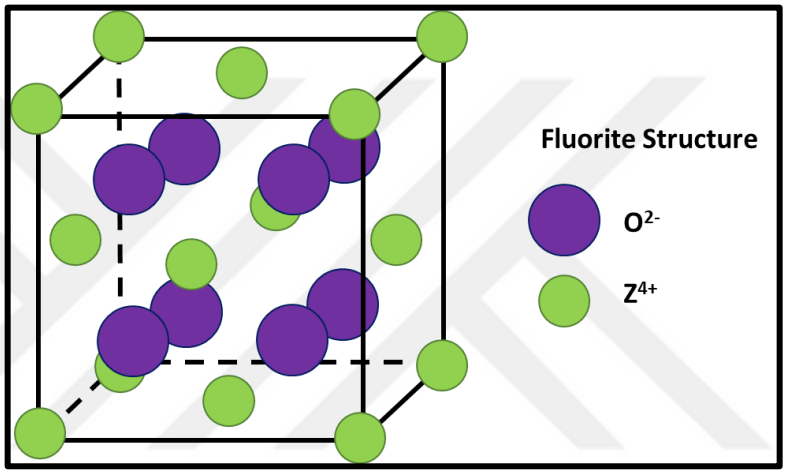

Figure 2. 3: Fluorite structure.

Various fluorite-type electrolyte materials exist, especially for intermediate temperature fuel cells, such as gadolinia doped ceria (GDC) or bismuth oxide-based electrolytes [9-13]. However, these materials have other shortcomings. For example, GDC undergoes a partial reduction under reducing conditions, causing Ce^{4+} to Ce^{3+} conversion, concomitant to the generation of electrons, which induces electronic conductivity. Bismuth oxide-based electrolytes with immense ionic conductivities (ca. 100 times that of YSZ), they are not preferred because of their tendency to i) undergo phase transformation under oxidizing conditions and ii) reduce down to bismuth metal in the fuel environment [12, 14-19].

3. COMMON SOFC PROBLEMS

Although solid oxide fuel cells are highly efficient electrochemical devices, they are not completely commercialized yet, mostly due to problems originating from their high operating temperatures (ca. 800-1000 °C). Some of the known changes caused by high operating temperatures are the microstructural and chemical degradations that take place at the electrodes, leading to performance loss [20-23]. A brief summary of these microstructural and chemical degradations will be provided in this section.

In SOFCs, perovskite-based materials with the ABO_3 stoichiometry are used as air electrodes (cathodes). In the ABO_3 structure, A and B sites are occupied by cations with 3+ valances, the latter being one of the transition metal oxides, e.g., Co, Fe, Mn and etc. The A-site is usually doped with a 2+ cation, most frequently Sr^{2+}, to generate electron holes and/or oxygen vacancies – both of which contribute to high electrocatalytic activity for oxygen reduction [24]. During long-term exposure to operating temperatures, segregation of Sr to form electrochemically inactive $SrO/SrOH_2$, causing electrochemical activity loss is observed [25, 26]. The driving force for this phenomenon is the mechanical strain caused by the larger dopant cation (Sr^{2+}) in comparison to that of the host (usually La^{3+}), while the segregation process is a thermally activated diffusional one [27, 28].

Coarsening of Ni particles exposed for a long-time to high operating temperatures has been reported for Ni-based composite anodes (most frequently, Ni-YSZ) [8, 21, 29]. This has been shown to reduce the TPB length, causing a diminished electrochemical performance [8, 21, 29].

Another anode-related SOFC issue is the redox intolerance of the Ni-based composites. It is expected that upon extremely long-term operation, the fuel supply to the anode will be interrupted [8]. In this case, Ni within the Ni-YSZ anode is oxidized to produce NiO, which is accompanied by a ca. 69% expansion in volume [8]. This expansion brings about significant mechanical stress, which cracks the YSZ network and, in many cases, induces mechanical failure of the whole cell [8]. It has been reported that low-temperature fabrication and the adoption of an electrolyte-supported SOFC

design, in which a thicker electrolyte layer serves as the mechanical support, can improve redox tolerance on Ni-based anodes [30, 31].

For practical applications, which require large amounts of power, several SOFCs are stacked together and connected in series via interconnects. There are several types of interconnect materials. The most powerful candidate for interconnects is the metal-based interconnects due to their low production cost and high electrical conductivity. Additionally, it is easy to process metals to obtain gas channels for fuel and oxidant feed. However, typical austenitic or ferritic steels suffer from rapid corrosion in an oxidizing environment when they expose SOFC conditions [32]. This, in turn, results in poor current collection and thus, performance degradation.

As mentioned earlier, the phenomena that induce performance degradation, namely, cation segregation, microstructural coarsening, redox cycling, high-temperature metal oxidation are all diffusion mediated. This suggests that the rates of these phenomena are thermally activated and lowering the operating temperatures would either reduce their rates or practically eliminate them completely. However, oxygen ion transport through the electrolyte and electrochemical reactions at the electrodes are also thermally activated and will slow down and yield poor performance when the operating temperatures are reduced. Therefore, the challenge we face here is to maintain acceptable performances even at reduced operating temperatures.

4. PROPOSED SOLUTIONS TO ADRESS SOFC ISSUES

The studies reported in the literature aiming at the development of SOFCs that operate at ≤650 °C can be categorized into four main groups. These groups are studies focusing on i) development of new electrode materials, ii) engineering of extremely fine electrode microstructures, iii) development of new electrolyte materials and iv) designing new SOFC configurations. A brief review of these studies is provided below.

4.1. Development of New Electrode Materials

The oxygen reduction reaction (ORR) that takes place at the cathode is the main limiting factor for the performance of the intermediate temperature solid oxide fuel cells (IT-SOFCs). When the generic p-type electronic conductor (La, Sr)MnO_3 (LSM) is used as the electrocatalyst, the ORR strictly occurs at TBP, the length of which firmly depends on the microstructure of the electrode. However, mixed ionic-electronic conductor (MIEC) materials that exhibit both electronic and ionic conductivity can be addressed as a solution to improve the low temperature performance of SOFCs. The mixed conducting nature of LSCF and its variants allow for the whole electrode surface to be electrocatalytically active and provide high surface exchange coefficient of oxygen [7]. Steele et al. measured the electrochemical performance of $La_{0.6}Sr_{0.4}Co_{0.2}Fe_{0.8}O_{3-x}$ (LSCF) as 0.18 Ω.cm² at 700 °C [33].

For example, Eksioglu et al. synthesized LSM single-phase and LSM-SDC nanocomposite cathodes via polymeric precursor deposition and surveyed its electrochemical performance at 600 °C. The results clearly showed that the polarization resistance of cathodes can be improved by the addition of the ionic phase. Polarization resistances of single LSM phase and LSM-SDC nanocomposite are 11.56 and 0.72 Ω.cm² at 600 °C, respectively [34].

4.2. Engineering of Extremely Fine Electrode Microstructures

Another approach to minimize the operating temperature of SOFCs is that preparing a mixing consists of electrocatalyst and electrolyte material to increase the TBP length. The results in the literature revealed that the performance of LSM cathodes can be improved by the addition of YSZ [35]. The conventional electrocatalyst-ionic conductor composite electrodes have been fabricated by the co-sintering of a powder mixture of respective phases at high temperatures (i.e., 900 - 1500 °C). However, these high temperatures required to ensure powder/powder and powder/electrolyte bonding causes particle coarsening resulting in retarded reaction kinetics due to reduced triple-phase boundary length [7, 36, 37]. For example, Fan et al. fabricated a composite cathode using a powder-derived method, coprecipitation, and glycine nitrate processing, with an electrocatalyst $La_{0.8}Sr_{0.2}MnO_3$ (LSM) and an ionic conductor $Ce_{0.9}Sm_{0.1}O_2$(SDC) ionic conductor powders [38]. The synthesized powders were fired at 1100 °C to obtain the desired microscale particle size. However, the obtained LSM – SDC composite cathode showed a poor polarization resistance as 0.47 Ω.cm² even though the impedance measurements were taken at 800 °C [38]. To overcome this issue, engineering of electrode microstructures to minimize the particle size of electrodes down to nanoscale has been another approach [7]. Here, the logic is that at lower operating temperatures, nanostructured electrodes cannot microstructurally coarsen and lead to performance degradation. One method to obtain nanocomposite electrode microstructures is the infiltration/impregnation of aqueous metal nitrate solutions into porous ionic conductor scaffolds, followed by low-temperature calcination (ca. 400 °C). For example, LSCF cathodes have been developed by infiltration into YSZ scaffold and they have 0.16 ohm.cm² polarization resistance at 700 °C [39]. NiO – YSZ anodes prepared by Ni infiltration has well-performed 0.25 ohm.cm² polarization resistance at 650 °C due to the impregnation of Ni enhances the catalytic activity and ionic conductivity of the electrode [40].

The low-temperature fabrication of Ni-YSZ anodes have also been reported to remedy the redox intolerance problem of these materials. The volume expansion of the Ni phase when converting to NiO upon an accidental (or intentional) interruption of the

fuel supply cracks the YSZ network within the anode, causing a significant performance loss [8, 29]. Furthermore, complete destruction of the whole cell has been reported in the case of anode-supported designs. The infiltration-based Ni-YSZ anode fabrication has been shown to result in anodes that can tolerate up to 15 reduction-oxidation cycles without performance loss in electrolyte supported designs, reportedly due to the low-temperature fabrication [30].

A more recently developed methodology has proven very effective to produce composite electrodes with nanoscale features. In this case, a single liquid precursor containing all the cations of both the electrocatalyst and ionic conductor phases is deposited on to a dense electrolyte substrate and heat treated at relatively low temperatures of 600-900 °C. Upon heat treatment the cations are expected to preferentially cluster to form their respective phases at nanoscale [34, 41, 42]. For example, Bilbey fabricated Ni-YSZ composites from a polymeric precursor containing all the cations of both Ni and YSZ phases [43]. She reported that the Ni-YSZ thin films had Ni and YSZ particle sizes below ca. 20 nm, which yielded a low polarization resistance of ca 0.75 $\Omega.cm^2$ at 600 °C [43]. Additionally, Eksioglu et al. reported that the single polymeric precursor-derived LSM-SDC cathodes had average particle sizes below ca 70 nm and exhibited an acceptable polarization resistance of 0.72 $\Omega.cm^2$ at 600 °C, in stagnant air [34].

4.3. Development of New Electrolyte Materials

Even if YSZ electrolytes are produced as thin as possible, their performance at low temperatures is not sufficient for the commercialization of SOFCs. The most powerful candidate against YSZ is the fluorite structured Bi_2O_3 due to its immense ionic conductivity that is ca. a hundred times that of YSZ [6]. However, in pure Bi_2O_3, the cubic bismuth oxide phase, which is the most ionic conductive phase, is known to undergo phase transformation at operating temperatures, in air [44, 45]. In the temperature between room temperature and foreseen operating temperature (<650 °C) the monoclinic bismuth oxide phase is stable [46]. To stabilize the high ionic conductive cubic bismuth oxide phase, rare earth oxide doping strategy was followed using Er_2O_3

and Y_2O_3 dopants, and these dopants yielded the cubic bismuth oxide phase at operating temperatures [12, 13]. Albeit the cubic phase exists in the range of 600-650 °C operating temperature, some studies revealed that full stabilization of cubic bismuth oxide using rare earth oxide dopants could not be possible due to the obtained cubic phase is metastable at operating temperatures but transformation kinetic of phase transformation from cubic to rhombohedral is sluggish [47]. The phase transformation causes conductivity decay upon long term operations [47]. A recent study investigated the dependence of conductivity decay and phase transformation when the Y_2O_3 doped Bi_2O_3 electrolytes exposure at operating temperature, in particular, is 650 °C [48]. They sintered YSZ-YDB electrolytes at different temperatures (at 800, 900, 1000, 1100 °C) and revealed that the sintering temperature of Bi_2O_3 electrolytes strongly affects the phase and conductivity stability and more stable samples obtained after high-temperature production (1000 and 1100 °C) [48]. Another conductivity decay mechanism was reported as anion order-disorder below 600 °C operating temperature and the proposed solution is the multi-doping strategy to provide slower ordering [49, 50]. Moreover, Fung et al. reported that the addition of ZrO_2 into Bi_2O_3 significantly mitigates (up to 3000 hours) the phase transformation at 600 °C [51]. Another unresolved issue about Bi_2O_3 is that forming of Bi metal when the electrolyte was exposed to IT-SOFC conditions. This situation has severely restricted integration of bismuth-based electrolytes in IT-SOFCs. The main approach to overcome this issue is that some non-reactive coating applications on the fuel side of bismuth oxide-based electrolytes and developing bi-layer electrolyte architect. A high amount of study reported that the OCV increment have been observed when a non-reactive coating is applied onto fuel side [52-55]. This OCV increment is associated with gas leakage-free fuel side coatings that ensure chemically stable Bi_2O_3 on the air side of bi-layer model [52-55].

4.4. Designing New SOFC Configurations

Development of new fuel cell designs and their processing are other areas of research that may succeed in lowering the operating temperature of these devices. The

electrolyte thickness is typically around 100-200 μm for electrolyte-supported cell designs when conventional YSZ electrolyte is used. However, to obtain lower ohmic resistances, YSZ electrolyte thicknesses below 10 μm is essential [7]. Even an electrolyte-supported cell was prepared properly with self-supported 20 μm thickness, the ohmic resistance was acceptable only over 700 °C [7]. To overcome this problem, cell designs using anodes as mechanical support have been proposed [5, 7, 56].

A successful attempt to develop IT-SOFCs has been made by the Wachsman group [57, 58]. They have developed and implemented a Ni-GDC anode-supported SOFC with a ca. GDC electrolyte [57, 58]. To enhance the relatively low OCV caused by the electronic conductivity of GDC induced by partial reduction at the anode side, a Er_2O_3 stabilized Bi_2O_3 coating with extremely high ionic conductivity and an oxygen transfer number of 1 in air, was applied at the cathode/electrolyte interface [58]. They have reported extremely high power densities of 1.94 Watts/cm^2 at 650 °C [58]. Meanwhile, no data on the long-term stability of this cell has been reported, to the best of our knowledge.

To obtain less resistive electrolytes a bilayer electrolyte models, such as YSZ/GDC or Bi_2O_3/GDC, have been proposed by a lot of research groups [57-60]. Especially, bismuth oxide/doped ceria design for electrolytes have shown good performance in the recent reviews due to the high ionic conductive bismuth oxide membrane [61-63]. Using GDC layer on the fuel side to prevent contact points of bismuth oxide with fuel, otherwise, the bismuth oxide reduces to Bi metal [62]. The bi-layer model ensures higher OCV values compared to single-layer ceria electrolytes and was stable for 1400 h when it was exposed to SOFC conditions [63].

5. AIM OF THIS THESIS

As mentioned earlier, for IT-SOFC applications, mostly, anode-supported designs, fabricated by tape-casting and co-sintering of anode and electrolyte layers have been proposed [5, 7, 56]. Despite the high performances, no reports exist on their long-term stability and redox tolerance. It is very likely that the thick anode layer will destroy the cell upon redo-cycling even at low temperatures [8, 64]

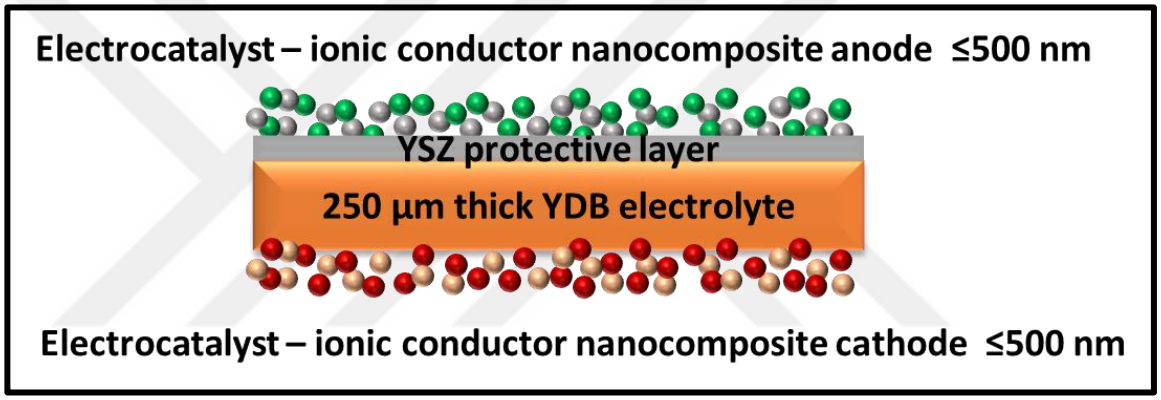

Figure 5. 1: Proposed electrolyte supported SOFC design.

In the present work, in order to i) avoid complete destruction of the cell upon redox cycling and ii) to allow for the use of the polymeric precursor-based nanocomposite electrode fabrication techniques an electrolyte supported design is adopted in the present case. Indeed, YSZ electrolyte had to be replaced by an alternative material with a significantly higher ionic conductivity, namely, Y_2O_3-doped Bi_2O_3 (YDB). However, it is well-known that Bi_2O_3 –based electrolyte materials reduce down to Bi metal when exposed to H_2 gas, under SOFC conditions [44, 45]. For example, Ahn et al. reported that open circuit voltage of an anode supported cell was improved from 0.73 to 0.77 V at 650 °C with an Er_2O_3 stabilized Bi_2O_3 (ESB) 4 µm-thick layer on a thick GDC electrolyte [57]. The enhancement of the OCV has been associated by the partial reduction of GDC has been blocked by ESB layer because of its high ion transference number [57, 58, 61]. Therefore, to render the YDB usable in our

electrolyte-supported SOFC, we propose to deposit a thin, dense YSZ coating onto the fuel-side of the YDB electrolyte. Despite the studies reporting deposition of a thin, Bi_2O_3 –based oxide onto thicker GDC or YSZ electrolytes [53, 57, 58, 61, 62], vice versa has never been reported to the best of our knowledge. This bilayer YDB/YSZ electrolyte-supported design (schematically shown in Figure 5.1) will also allow for the utilization of the polymeric precursor-based nanocomposite electrode fabrication route.

Here, it was aimed to fabricate YDB/YSZ bilayers with that are applicable to electrolyte supported IT-SOFCs. We have especially focused on the methodology to fabricate i) ca. 200 µm, dense YDB substrate via power synthesis, tape casting and sintering methods and ii) thin, crack-free YSZ films by a cost-effective and facile polymeric precursor technique. The effect of polymeric YSZ precursor deposition conditions on the thickness, crack formation and hydrogen blocking properties were thoroughly investigated.

6. EXPERIMENTAL

6.1. Preparation of Dense YDB Electrolytes

6.1.1. Powder Synthesis

28% mol yttria doped Bi_2O_3 (YDB) powders were synthesized by a modified Pechini method using yttrium (III) nitrate hexa-hydrate (Alfa Aesar, 99.8% trace metal basis) and bismuth (III) nitrate penta-hydrate (Alfa Aesar, ACS reagent ≥98.0%) metal salts. These salts were dissolved in stoichiometric amounts in de-ionized water and nitric acid mixture (1:1 wt ratio) until clear solution was obtained. Ethylene glycol was added into the clear solution that has been heated up to 200 °C and stirred for 24 hours. After 24 hours of stirring, a viscous, polymeric gel was obtained. The produced gel was heat treated at 700 °C for 4 hours to eliminate nitrate compounds and obtain the desired fluorite phase. To achieve a monodisperse particle size distribution, ball milling was performed. For milling, 6.5 grams of synthesized YDB powders were mixed with a certain amount of ethanol (75 grams) and ZrO_2 milling media (100 grams) in a 250 ml PTFE bottle and milled for 24 hours at 180-200 rpm. The powder - ethanol mixture was dried in an oven at 120 °C for 3-4 hours, before consolidation into YDB substrates.

6.1.2. Consolidation and Sintering of YDB Powders

Green YDB pellets were prepared via uniaxial die pressing at 1.7 MPa. Afterward, substrates were held in a cold isostatic press for 2 min under 200 MPa. Consolidated YDB substrates were held at 900, 1000 and 1100 °C for 6 hours to achieve dense and 800 µm-thick sintered samples. Sintered samples are encoded as YDB-900, YDB-1000, YDB-1100 according to their sintering temperatures.

The synthesized dry powders were also consolidated into planar samples by tape casting. Obtained 25 grams dry YDB powders were mixed with a binder mixture that is

consisting of 30.43 grams toluene and 14.13 grams ethanol as solvents, 3.62 grams polyvinyl butyral (PVB) as a binder and 1.81 grams dibutyl phthalate (DOP) as a plasticizer. Prepared binder mixture was added into a 150 ml PTFE bottle and 200 grams of ZrO_2 milling media was also used to provide well-dispersed and homogenous mixing. The tape slurry was milled for 24 hours at 180-200 rpm, as well. Well-dispersed tape slurry was cast onto Mylar sheets using a doctor blade. Blade gap was selected as 400 µm to obtained single-piece green YDB tapes onto a Mylar sheet (obtained Polinas, Turkey). The tape slurry was dried out at room temperature until flexible 320 µm-thick green YDB tapes were obtained. The sintering of green tapes was performed at 1000 °C for 6 hours with a heating rate of 5.8 °C per minute. The sintered dense YDB tapes had roughly 220-250 µm thicknesses.

6.2. Preparation of YSZ Polymeric Precursors and Their Deposition on YDB Ceramics

Since the starting materials used to prepare the polymeric 8 mol% Y_2O_3 stabilized ZrO_2 (YSZ) solutions are expected to have a great impact on the degree of polymerization and hence, the quality of the YSZ coatings to be deposited onto the YDB ceramics, we have tried four different types of polymeric YSZ precursors in the present study. The most important parameter was determined as the degree of polymerization, therefore, the generic polymeric YSZ precursor was modified by i) adding nitric acid to facilitate the conversion of ethylene glycol into oxalic acid, the main chelating agent in the Pechini-type process [65] ii) switching the generically used zirconium source from zirconyl chloride octahydrate to zirconium oxynitrate hydrate and thereby releasing nitric acid into the solution from the zirconium source, instead of hydrochloric acid. Following this logic, four types of precursor solutions were prepared. The first type of the YSZ precursor was the same as those prepared for the purposes of infiltration into porous scaffolds in [31] and [66]. Basically, appropriate amounts of yttrium (III) nitrate hexahydrate (Alfa Aesar, 99.8% trace metals basis) and zirconium oxychloride octahydrate (Sigma Aldrich, %98 reagent grade) were dissolved in a mixture of distilled water and ethylene glycol, then stirred at 120 °C until all water had evaporated and

polymerization took place. The other two types of polymeric YSZ precursors were prepared by adding nitric acid to the clear solution during the polymerization process in amounts that would yield ethylene glycol to nitric acid weight ratios of 2:100 or 4:100. The fourth type of polymeric YSZ precursor was prepared by the same method, except the zirconium source was switched from zirconium oxychloride octahydrate (Sigma Aldrich, %98 reagent grade) to zirconium oxynitrate hydrate (Sigma Aldrich, %99 anhydrous basis) and no additional nitric acid was added. After the polymerization process, all the precursors were diluted with 2-butoxyethanol in an equivalent amount to the polymeric precursor to reduce the overall surface tension and facilitate wetting. The main parameters of the four different polymeric precursors along with the sample codes are provided in Table 6.1.

The deposition of the prepared polymeric precursors was realized by a dip-coating process using withdrawal rates of 100 mm/min and 150 mm/min. After the deposition, the samples were heated up to 350°C at a heating rate of about 12.5 °C per minute until all solvents and organics were eliminated. Then, the hot plate is turned off and the sample is left to cool down to room temperature, which takes about 30 minutes. To achieve the desired film thicknesses, the deposition/drying cycles were repeated for 5-7 times.

Table 6.1: Key contents of the different YSZ precursors and the corresponding codes.

Solution code	**Zr source**	**Y source**	**Nitric acid:ethylene glycol (weight ratio)**
YSZ-Cl-0N	zirconium oxychloride octahydrate	yttrium nitrate hexahydrate	0
YSZ-Cl-2N	zirconium oxychloride octahydrate	yttrium nitrate hexahydrate	2:100
YSZ-Cl-4N	zirconium oxychloride octahydrate	yttrium nitrate hexahydrate	4:100
YSZ-N-0N	zirconium oxynitrate hydrate	yttrium nitrate hexahydrate	0

Deposition of the YSZ thin films was realized using dip-coater with withdrawal rates 100 and 150 mm/min for YDB pellets and sintered tapes, respectively. Deposited YSZ thin films were heated up to 350 °C at a heating regime of about 12.5 °C per

minute on a hot plate. Afterward, the hot plate was turned off and the deposited samples were held on hot plate until the hot plate was cooled down to room temperature, which takes about 20-30 min. Heating-up process was realized to provide elimination of solvents and organics from deposited polymeric precursors. To achieve the appropriate film thickness for blocking layer applications, deposition process was repeated for 5-7 times.

6.3. Materials Characterization

The microstructural characterization of the samples was performed by scanning electron microscopy (SEM – Philips XL 30 S FEG) with an energy dispersive x-ray spectroscopy attachment (EDX – EDAX Amatek Apollo XPP) that was used to determine the elemental distribution in the prepared samples. The crystal structure of sintered YDB ceramics and investigation of possible chemical reaction between YSZ polymeric precursor and YDB substrates were analyzed by x-ray diffraction (XRD) analyses performed at a 2θ range of 20 - 80 ° using Cu K_α characteristic radiation (Rigaku D/max 2200). YSZ dry-gels have been prepared on hot plate at 120-150 °C for XRD analyses and mixed with YDB powders that were heat treated at 1000 °C to be able to demonstrate sintered YDB ceramic conditions, to avoid the signals that may come from YDB substrates due to extremely thin (<500 nm) YSZ films.

Electrical conductivity of the YSZ/YDB bilayer electrolytes was determined by impedance spectroscopy measurements. Here, the term impedance is used to describe the resistance under alternative current (AC) flow, basically. Electrochemical impedance is measured by applying a sinusoidal excitation potential to an electrochemical cell. This excitation voltage is mathematically describing in Equation 6.1, where E_t shows the potential value at a certain time (t), E_0 is the excitation voltage and ω is the radial frequency. In turn, a sinusoidal current, with a phase shift (ϕ) is generated, as mathematically described in Equation 6.2.

$$E_t = E_0 \sin(\omega t) \quad (6.1)$$

$$I_t = I_0 \sin(\omega t + \phi) \quad (6.2)$$

The impedance of the system can be calculated with equation 6.3.

$$Z = \frac{E_t}{I_t} = \frac{E_0 \sin(\omega t)}{I_0 \sin(\omega t + \phi)} = Z_0 \frac{\sin(\omega t)}{\sin(\omega t + \phi)} \quad (6.3)$$

We also can apply Euler's relationship on that sinusoidal functions,

$$\exp(i\phi) = \cos\phi + i\sin\phi \quad (6.4)$$

The impedance value of the system can be represented as a complex number,

$$Z = \frac{E}{I} = Z_0(cos\phi + i\sin\phi) \quad (6.5)$$

The graph obtained using Equation 6.5 is known as the Nyquist plot and consists of the real and imaginary parts of the impedance value. In Nyquist plot, phase shift represents the angle between x-axis and absolute value of Z. The typical Nyquist plot is represented in Figure 6.1. Here, R_1 is the ohmic resistance, dominated by the oxygen ion transport through the electrolyte and any current collection losses, while R_2 is the total electrode polarization resistance, induced by the oxygen reduction/hydrogen oxidation processes. Therefore, in our electrical conductivity measurements, we assumed that R_1 gives the resistance to oxygen ion transport through the bilayer electrolyte. The electrical conductivity is then given by:

$$\sigma = \frac{l}{A.R_1} \quad (6.6)$$

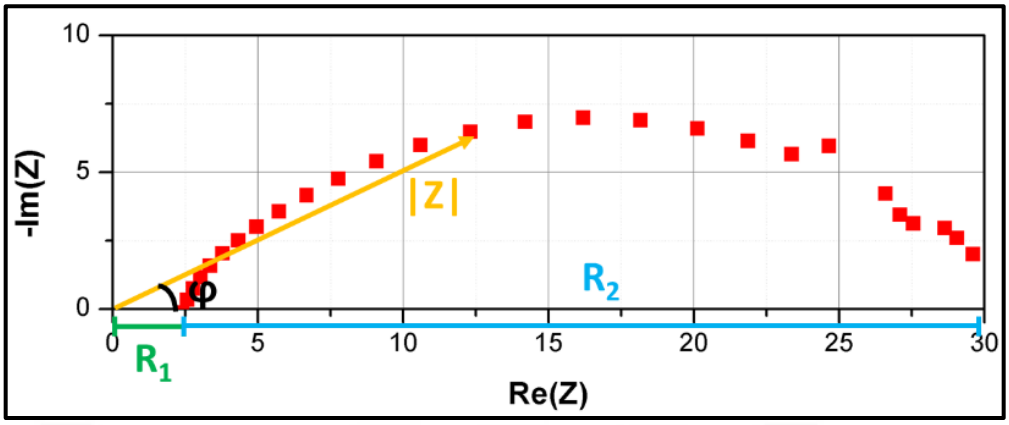

Figure 6. 1: A typical Nyquist graph.

For electrical conductivity measurements performed in samples with symmetrical half-cell configuration (Ag current collector/YDB/YSZ/Ag current collector) Biologic SP-150 was used. Ag current collectors were deposited via brush-painting onto both sides of the developed bilayer electrolytes using our in-house Ag current collector paste [67]. Two Ag wires were attached onto Ag current collector covered surfaces using a ceramic adhesive (Ceramabond 503, Aremco, USA) for high temperature applications. EIS measurements were performed at a temperature range of 400 – 600 °C, in stagnant air, and 10 mV excitation voltage was applied to system at the frequency range of 10^{-1} – 10^{5} Hz.

Blocking properties of the YSZ thin films in the prevention of the transformation of Bi_2O_3 into metallic Bi when it exposes to SOFC conditions was investigated by open circuit voltage (OCV) measurements using another potentiostat (Gamry Reference 3000 potentiostat/galvanostat/EIS analyzer). Open circuit voltage measurements were performed at 600 °C, under the flow of a humidified gas mixture of 10% H_2 – 90% Argon to fuel side of the YDB/YSZ bilayer electrolytes. A dense and leakage-free Al_2O_3 tube was used to build up an experiment system to separate air and hydrogen sides of the system. Prepared bare YDB and bi-layer electrolytes were sealed onto alumina tube using same ceramic adhesive conducting Ag wires and held at room temperature until the adhesive had been dried. Afterward, a glass sealant (Ceramabond 569, Aremco, USA) was applied onto ceramic adhesive to ensure gas tightness.

6.4. Fuel Cell Measurements

Fuel cell measurements were performed under same gas mixing flow that had been used in OCV measurements. Electrode selection has been done according to performance values of the electrodes that had been optimized in our research group [43, 68]. $La_{0.8}Sr_{0.2}MnO_3$-$Bi_{0.72}Y_{0.28}O_{1.5}$ (LSM-YDB) composite electrode was selected as a cathode material and NiO-$Ce_{0.8}Gd_{0.2}O_2$ (NiO-GDC) composite electrode was selected as an anode material.

Production of LSM-YDB composite cathodes depends upon the separate production of LSM and YDB polymeric precursors and mixing of these solutions in a certain amount. To prepare LSM polymeric precursor, lanthanum (III) nitrate hexahydrate (Fluka), strontium nitrate (Sigma – Aldrich) and manganese nitrate hexahydrate (Sigma – Aldrich) have been dissolved in distilled water until clear solution had been observed, then ethylene glycol was added and the solution stirred at 80 °C until all water had evaporated and polymerization had completed. The preparation route of YDB polymeric precursor had been discussed in previous chapter. However, the prepared nitrate salts containing polymeric solution stirred at 80 °C instead of 200 °C to ensure complete polymerization and to obtain clear polymeric precursor. Obtained LSM and YDB polymeric precursor were mixed with each other in a 60:40 volume ratio, respectively.

Nanostructured NiO – $Ce_{0.8}Gd_{0.2}O_2$ (NiO-GDC) anode precursors were prepared in a similar way with LSM-YDB composite cathode precursor. To prepare NiO polymeric precursor, firstly, nickel nitrate hexahydrate (Sigma – Aldrich, crystals or chunks) was dissolved in deionized water until clear solution had been obtained. Then, ethylene glycol was added into clear solution that stirred at 80 °C until all water had evaporated, and polymerization took place. Preparation of GDC polymeric precursor was realized in the same route using cerium nitrate hexahydrate (Alfa Aesar, 99.5%) and gadolinium trinitrate hexahydrate (Alfa Aesar ≥ 99.9%). NiO and GDC polymeric solutions were prepared separately and mixed with each other in a 60:40 volume ratio, respectively.

Resultant electrode precursors were deposited onto sintered YDB tapes by a dip-coating method using a withdrawal rate 150 mm/min. After each deposition, YDB ceramics were held on a hot plate that was heated up to 350 °C to eliminate organics from the deposited polymeric precursor. Then, the hot plate was turned off until surface of the hot plate reached to 50 °C. To obtain appropriate electrode thickness, the deposition route was repeated 5 times on each side.

Electrochemical measurements of prepared fuel cells, which have NiO-GDC/YSZ/YDB/LSM-YDB fuel cell architect, were performed under 10% H_2 – 90 Ar gas mixing flow at a temperature range of 500-600 °C. During the electrochemical measurements, three type methods were used to determine resistance values, power density and contribution on open circuit voltage of fuel cell. These were impedance spectroscopy, linear sweep voltammetry and open circuit voltage measurements, respectively. Electrochemical impedance spectroscopy measurements were performed at 10^4 – 10^{-1} Hz frequency range under 0.3 V polarization voltage (Gamry Reference 3000). A method like that used in the bi-layer electrolyte model has been followed in making the fuel cells suitable for electrochemical measurements.

7. RESULTS AND DISCUSSION

7.1. Long-term Electrical Conductivity Measurements of YDB Ceramics

It is well-known that the immense ionic conductivity of YDB ceramics is not stable at the intermediate operating temperatures. The reason for that is anion ordering and phase transformation of YDB at intermediate temperature range. Anion ordering has been reported in the literature for lower temperature (<600 °C), however, the phase transformation has been observed higher than 600 °C. Therefore, the conductivity degradation demeanors of YDB ceramics were investigated in this study at 600 °C for 100 h. YDB-900, YDB-1000 and YDB-1100 encoded samples were held at 600 °C and their ionic conductivity was monitored (Figure 7.1).

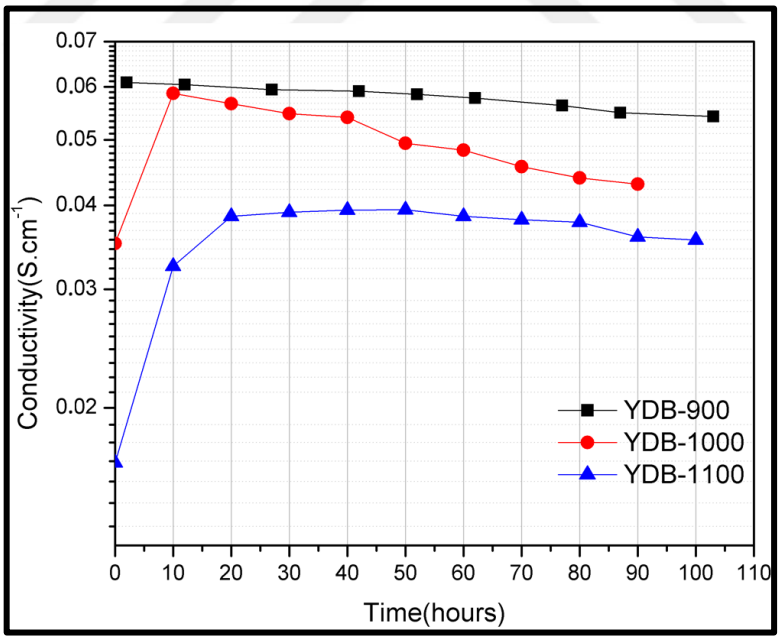

Figure 7. 1: Long-term conductivity decay of YDB ceramics sintered at different temperatures.

The electrical conductivity of YDB-900 and YDB-1100 remained more stable at 600 °C. In this study, we selected YDB-900 and YDB-1000 encoded samples for the deposition of YSZ thin films.

7.2. Microstructural Analysis of YSZ Coatings

One of the main objectives of this study to fabricate dense, continuous, and crack-free YSZ thin films on YDB substrates. YSZ thin films prevent the reduction of YDB ceramics by preventing their contact with hydrogen gas. For this purpose, YSZ thin films deposited on YDB ceramics using a cost-effective and facile polymeric precursor method. In the literature, a generic YSZ polymeric precursor was used for infiltration processes of electrodes for SOFC applications. In this study, initial deposition processes were performed with the same polymeric YSZ precursor which contained zirconium oxychloride hydrate and yttrium nitrate as Zr and Y sources, respectively. This generic polymeric precursor was used a lot of time for infiltration into porous electrode materials to ensure longer triple-phase boundary [31, 39, 66]. In fig 7.2a shows the crack formation of YSZ thin films on YDB ceramics. Although there is a thermal coefficient difference between YSZ and YDB (20.3×10^{-6} and 7.8×10^{-6} for YDB and YSZ, respectively) [69, 70], relatively thin YSZ films (< 500 nm) and crack formation even at low temperatures (thin films only were exposed to a maximum of 380 °C), show that the crack formation is related to precursor formation mechanism-related situation.

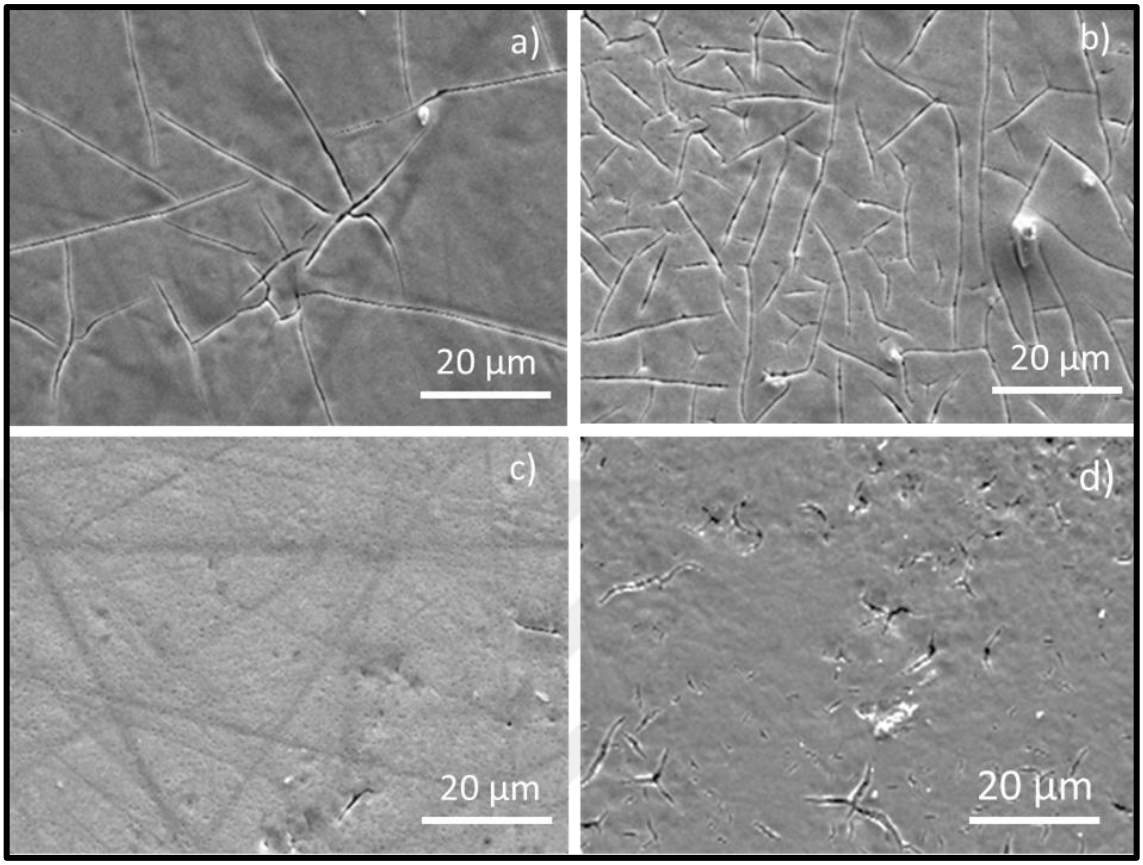

Figure 7. 2: The top surface scanning electron microscopy images of dip-coated YDB ceramics using a)YSZ-Cl-0N, b)YSZ-Cl-2N and c)YSZ-Cl-4N solutions in the as-deposited/dried state, d) YSZ-Cl-4N coating heat treated at 600 °C for 4h.

Chen et al proposed that the ethylene glycol was catalyzed by the nitric acid in solution and converted to oxalic acid [71]. So, the addition of nitric acid into the polymeric precursor ensures the chelation of metal ions in the polymeric precursor. That process takes place during stirring and heating on a hot plate. The illustration of the formation of vanishing cracks in the PEG containing coatings are given in Figure 7.3. In the case of figure 7.2a, nitric acid addition was not used to form the polymeric precursor during stirring. Therefore, the possibility of the existence of uncompleted organic forms in the deposited thin film can be caused crack formation due to their thermal expansion difference from the YDB substrate and completely polymerized YSZ thin films. Additionally, in case of existence of the proper amount of nitric acid in polymeric precursors could cause completely oxidized ethylene glycol. However, there is another possibility for the evolution of polyethylene glycol (PEG) during the precursor

fabrication process. Some results have been reported that if there are PEG in precursor-derived thin films, PEG can decompose and forms crack during the heat treatment process [72, 73]. At this point, the addition of nitric into polymeric precursors must reduce or eliminate crack formation in thin films.

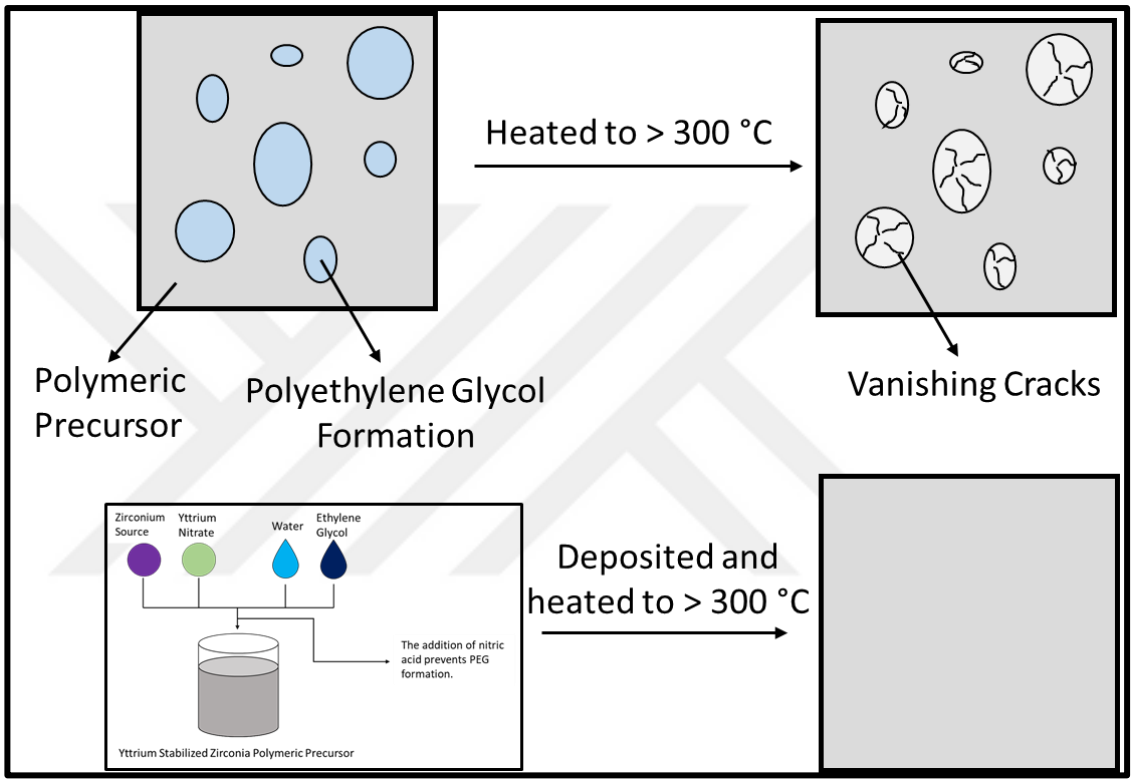

Figure 7. 3: Demonstration of the effect of the nitric acid addition on the thin films.

Fig 7.2b and c show the surfaces of deposited thin films these are derived from other polymeric precursors with increasing nitric acid amounts (YSZ-Cl-2N and YSZ-Cl-4N), in the as-deposited state. The cracks became shorter and narrower when the nitric acid was added. If the amount of nitric acid was doubled, it was observed that the cracks were eliminated completely. Since YDB/YSZ bilayer electrolytes are exposed to SOFC conditions, fig 7.2c shows the surface image of the YSZ thin film, whose deposited state has been optimized, after heat treatment at 600 °C for 4 h. Heat-treated YSZ thin films had small and isolated cracks. One possible reason for these cracks is the removal of some organics from thin films in the gaseous phase because of high temperature heat treatment. For example, graphitic carbon might have been removed as

a result of polymer decomposition at 600 °C, in air [73]. Alternatively, any dimensional change upon heat treatment at the YDB/YSZ interface might also have caused crack formation because of occurring reactions between the substrate and thin film.

To further test our hypothesis, we prepared another solution but switching Cl containing Zr source that does not release nitric acid-forming ions to the solution with nitrate containing Zr solution to investigate oxalic acid evolution with not adding nitric acid into the prepared polymeric precursor. This way, the ions released from nitrate containing Zr source behave like nitric acid addition and employed in the oxalic acid formation. Fig 7.4 shows the surface SEM images of the YDB ceramics deposited with YSZ-N-0N solution and after 4 h of heat treating at 600 °C, respectively. No visible cracks were observed (only a few scratches originating from substrate polishing) in the as-coated state of YSZ thin films (Figure 7.4a). The crack-free structure of YSZ-N-0N after holding at 600 °C (Figure 7.4b) is also promising. These results confirmed our hypothesis about oxalic acid formation with the addition of nitric acid.

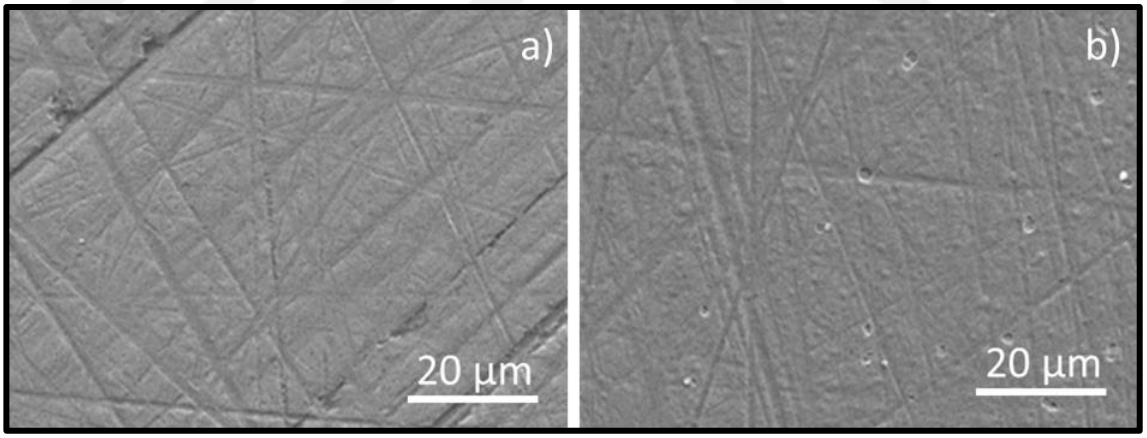

Figure 7. 4: Scanning electron microscopy images of YDB substrates coated using YSZ-N-0N solution a) in the as coated/dried state and b) after heat treatment at 600°C for 4 h.

7.3. Structural and Chemical Characterization

XRD analyses were performed in order to determine whether i) the desired fluorite crystal structures could be obtained from YSZ thin films and YDB substrates and ii) if any reactions occur at YSZ/YDB interface upon heat treatment (Figure 7.5). The

targeted fluorite structure has been obtained after sintering the synthesized YDB powders at 1000°C and calcining gels dried from the YSZ-Cl-0N and YSZ-N-0N precursors with YSZ phases having lower crystallinity because of the low-temperature heat treatment (Figure 7.5). To investigate any possible reaction that has taken place between YDB and YSZ, XRD analyses were also performed on mixtures of YSZ gels dried from different solutions, YSZ-Cl-0N or YSZ-N-0N, and YDB after heat treatment at 600 °C. Figure 7.5 shows that tetragonal Bi_2YO_4Cl formed when YSZ-Cl-0N was used, while separate YSZ and YDB peaks were visible when YSZ-N-0N was used as the YSZ precursor. The individual existence of Bi_2YO_4Cl peaks could cause crack formation at the surface of YSZ coatings derived from YSZ-Cl-4N after annealing at 600 °C due to molar volume difference between Bi_2YO_4Cl (79.47 cm^3/mol), YSZ (57.22 cm^3/mol), and YDB (51.98 cm^3/mol).

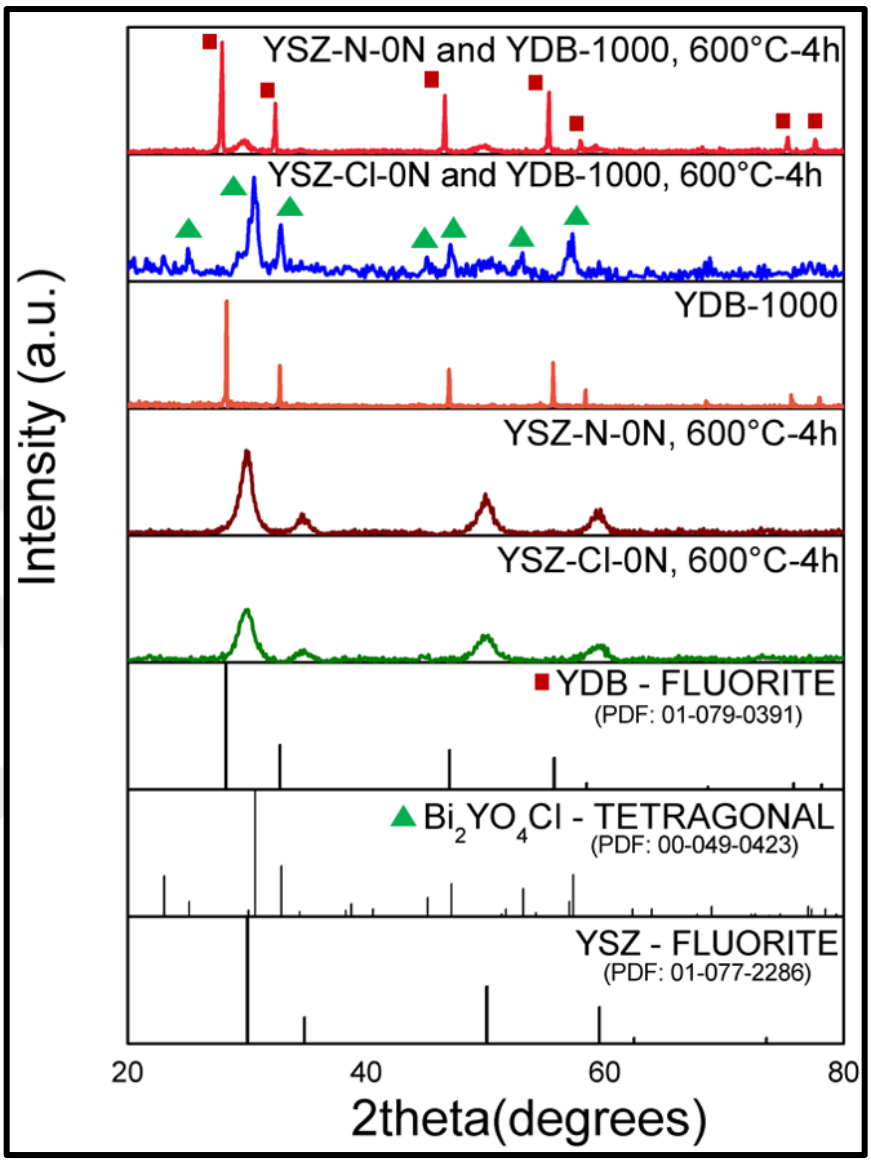

Figure 7. 5: X-ray diffraction patterns of YDB powders at calcined at 1000 °C, gels dried from YSZ-Cl-0N, YSZ-N-0N, mixtures of YDB – YSZ-Cl-0N and YDB – YSZ-N-0N all heat treated at 600 °C.

To determine whether any reaction occurred between YDB substrates and YSZ thin films derived from YSZ-Cl-4N and YSZ-N-0N, after heat treatment at 600 °C for 4 h and to evaluate film thicknesses SEM-EDX analyses were performed on the cross-sectional areas of the dictated samples (Figure 7.6). In Figure 7.6a, the film thickness is roughly 420 nm and a continuous, dense film was obtained on YDB ceramics. In SEM-EDX analyses, the thin films consist of while the dense substrate contains Bi and Y (Figure 7.6). Even though the Zr signal comes from the substrate, the concentration

gradient looks like an interdiffusion profile are likely because of the overlap of the L peaks of Zr and Y (Figure 7.6). A study revealed that the slurry-based bismuth oxide powders deposited onto YSZ electrolytes and heated up to 800 °C, there is no interdiffusion between substrate and coating [53]. Therefore, the coming Zr signals from the substrate is suggested as just a background. In Fig 7.6a, the Cl elements clusters have been observed these were close to the YSZ/YDB interface. The evolution of Cl clusters is agreement with the XRD results which show the Bi_2YO_4Cl formation when YSZ-Cl-4N derived precursor used (Figure 7.5). Furthermore, the presence of oxygen deficit regions causes Bi clustering into the substrate which is suggesting the formation of metallic bismuth when it exposes high temperature even in an air atmosphere (Figure 7.6a).

In the SEM image of figure 7.6b, the fracture surface of YSZ-N-0N derived YSZ thin film deposited YDB substrates depicted and 220 nm thick-film was observed despite using the same cycle deposition route with YSZ-Cl-4N derived precursor. Evidently, there are no observed Cl clusters (Figure 7.6b). Although the used polymeric precursor did not consist of any Cl containing raw material, there are visible Cl signals in the substrate that associated with overlaps of M and K peaks of Bi and Cl, respectively.

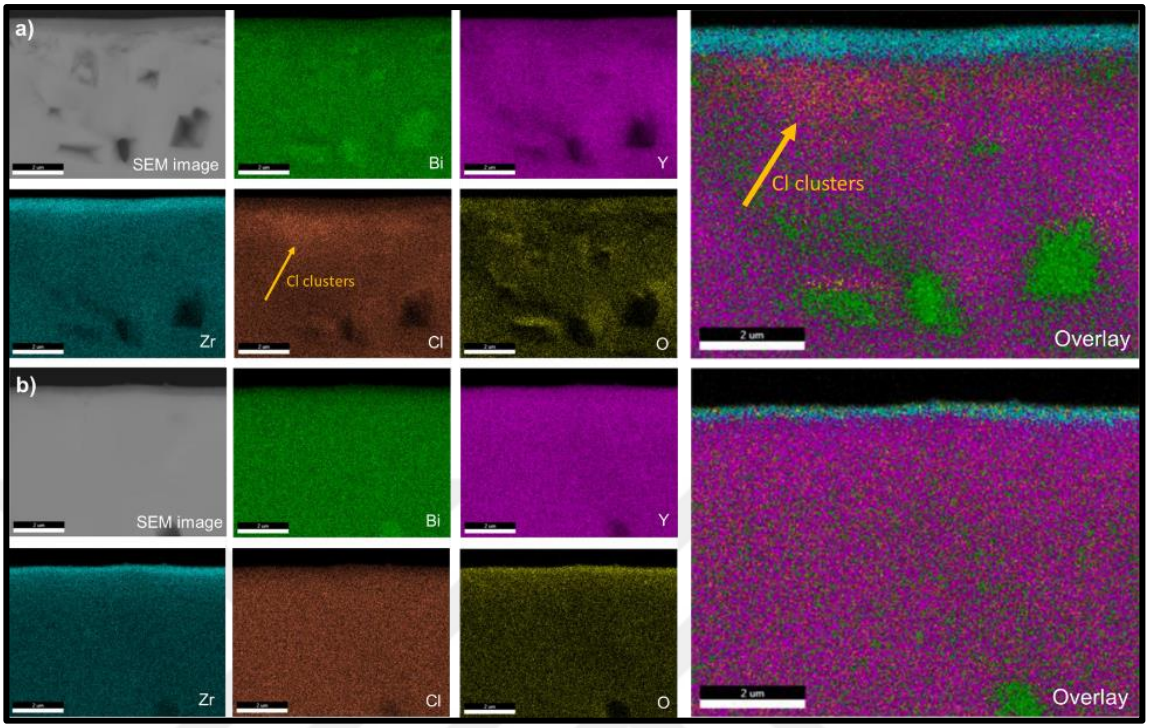

Figure 7. 6: SEM images and the corresponding EDX maps of a) YDB-1000 and b) YDB-900 ceramics dip-coated using polymeric YSZ-Cl-4N and YSZ-N-0N precursors, respectively. The scale bars represent 2 µm.

7.4. Electrochemical Characterization

To determine the resistance contribution of YSZ layers to total ohmic resistance, electrochemical impedance spectroscopy (EIS) analyses were performed on YSZ-Cl-4N coated YDB-1000, bare YDB-1000, and YSZ-N-0N coated YDB-900, bare YDB-900 (Figure 7.7). The first intercept of the horizontal axis and Nyquist curves represents ohmic resistance per specific area of the system in our scenario we encoded them as $ASR_{ohmic,\ YDB}$, and $ASR_{ohmic,\ YDB+YSZ}$ for substrate and thin film, respectively (Figure 7.7). For YSZ-Cl-4N derived coatings, ASR value increased from 1.44 to 12.67 ohm.cm² while for YSZ-N-0N derived coatings was increasing ASR value from 1.18 to 12.51 ohm.cm² (Figure 7.7). Furthermore, the electrical conductivities (σ) of coated YSZ layers were determined by a subtraction method using equation 7.1 with the thicknesses of the thin films (l_{ysz}). The electrical conductivities of thin films derived from YSZ-Cl-4N and YSZ-N-0N are 3.74 x 10^{-6} S/cm and 1.94 x 10^{-6} S/cm at 600 °C,

respectively. These values are somewhat lower than the expected conductivity values of the YSZ electrolytes [74]. However, the lower conductivity of the thin film was associated with lower crystallinity that corresponding to XRD data in figure 7.5. For example, Petrovsky et al. represented that the temperature dependence of the conductivity of YSZ thin films which were produced in the same method, polymeric precursor, and they reported that when the heat treatment temperature increases, conductivity would increase [74].

$$\sigma_{YSZ} = \frac{l_{ysz}}{(ASR_{ohmic,\ YSZ+YDB} - ASR_{ohmic,\ YDB})} \tag{7.1}$$

In the literature, studies on the bi-layer electrolyte system do exist in many cases uses bismuth oxide-based electrolytes as one of the electrolytes. Findings have shown that the additional resistance was not observed in GDC/ESB [58], SDC/ESB [57], and YSZ/ESB [53] contrary to the expected aspect. These results are associated with using a thinner bismuth oxide layer onto a zirconia or ceria layer instead of using bismuth oxide as a mechanical support and the main electrolyte. Therefore, a more conductive bismuth oxide layer has not much contribution to total ohmic resistance. In this study, we used bismuth oxide layer not only main electrolyte but also mechanical support in our electrolyte supported SOFC model, therefore, the additional resistance of YSZ on total resistance more detectable due to its low electrical conductivity.

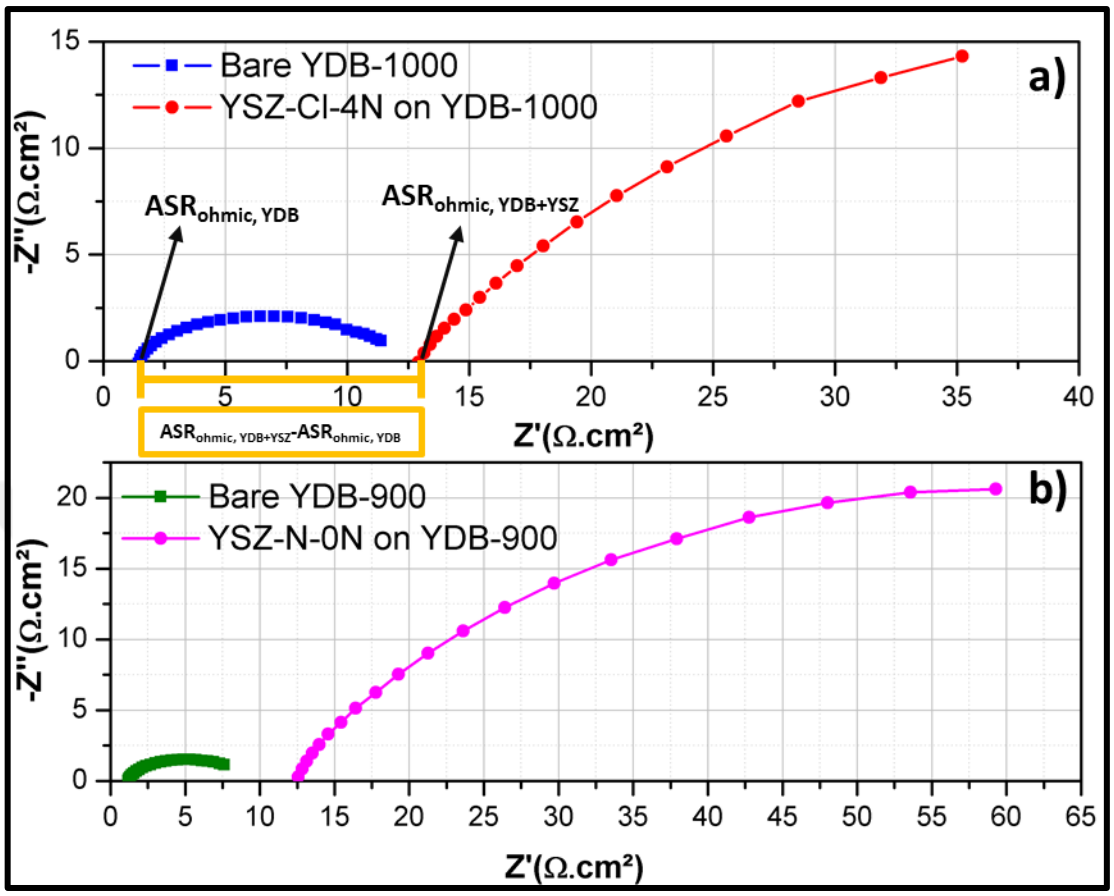

Figure 7. 7: Nyquist graphs obtained from a) bare and YSZ-Cl-4N deposited YDB-1000, b) bare and YSZ-N-0N deposited YDB-900.

Open circuit voltage (OCV) measurements were performed to YDB/YSZ bi-layer and bare YDB electrolytes to investigate blocking properties of developed YSZ overlayer, under 10% H_2 – 90% Ar gas mixing flow upon long term at 600 °C (Figure 7.8). For these measurements, YSZ-N-0N polymeric precursor derived coatings were used on YDB ceramics due to their crack-free and continuous nature. Some studies supposed that the thickness ratio of layers in bismuth oxide-based bi-layer electrolytes strongly affects the situation of bismuth oxide reduction into metallic Bi [58, 75]. For example, Lee et al. reported the deposition of bismuth oxide onto a relatively thick GDC layer causes higher OCV values at operating temperatures [58]. They also reported that when they former rearrange thickness ratios of ESB/GDC layers 1 to 2 the latter 1 to 12 they observed increased OCV from 0.82 to 0.92 V at 600 °C [58]. All of these studies reported their results for coated thin bismuth oxide electrolytes on relatively thick ceria

or zirconia-based electrolytes. In this study, we have focused on performing electrochemical measurements on YDB electrolytes with thin YSZ overlayers deposited by the polymeric precursor method. To provide high OCV, relatively thin YDB tapes (tape thickness ca. 220 µm) were used as substrate. Evidently, bare YDB ceramic could not retain its initial OCV value, which is 0.65 V, due to the reduction of Bi_2O_3 into metallic Bi after 10 h fuel flow (Figure 7.8). In contrast, the YSZ-N-0N precursor derived YSZ coated YDB substrates slightly increased the initial OCV value to 0.68 V (Figure 7.8). The OCV value remained at 0.62 V during the rest of the experiment and that is evidence of the effectiveness of the YSZ thin layer under fuel conditions.

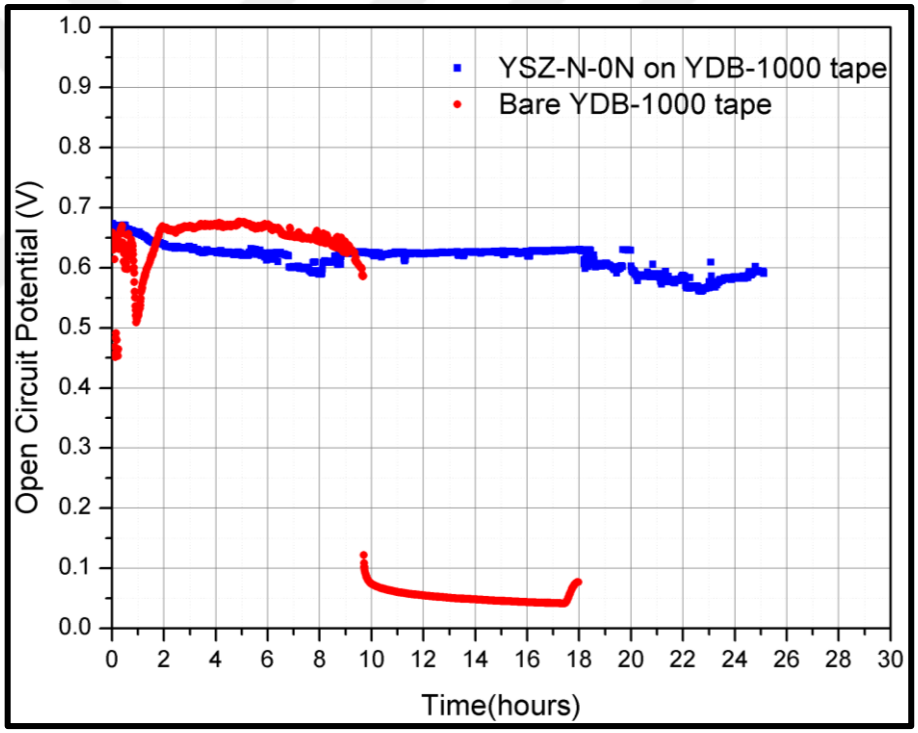

Figure 7. 8: Changes in open circuit voltages of a) bare YDB-1000 tape ceramic and b) YSZ-N-0N precursor derived YSZ deposited YDB-1000 tape at 600°C under fuel flow.

To further our experiment and to obtain low resistive bi-layer electrolyte for our electrolyte supported SOFC systems, the EIS measurements were performed also on sintered 250 µm-thick YDB-1000 electrolyte and YSZ-N-0N derived thin film coated YDB-1000 bi-layer (Figure 7.9). In this measurement, ASR values increased from 1.13

to 3.34 ohm.cm². The ASR values less increased in the tape-used-bi-layer model contrary to obtained EIS data from YSZ-N-0N derived thin films on YDB-900 (Figure 7.7b and Figure 7.9). According to Nyquist graphs of the tape-used-bi-layer model, the electrical conductivity of YSZ-N-0N derived thin films is 9.95 x 10^{-6} S/cm at 600 °C in stagnant air and that value is somewhat higher than the electrical conductivity of YSZ-Cl-4N derived thin films. The difference between electrical conductivities of YSZ-N-0N derived thin films on the different types of the substrate can be explained with surface roughness difference between tape and YDB pellets that could ensure a better contact area for EIS measurements.

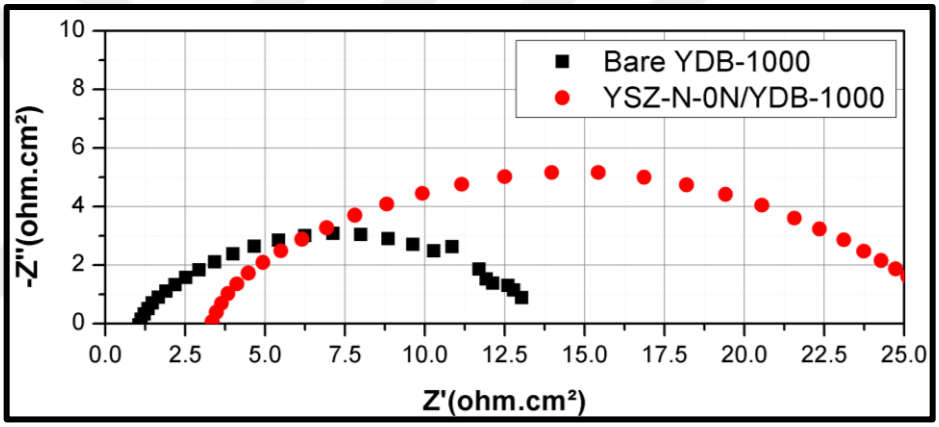

Figure 7. 9: Nyquist graphs of YDB-1000 tape and YSZ-N-0N/YDB-1000 bi-layer electrolytes.

As the final step in this study, we have constructed solid oxide fuel cells with YDB-YSZ bilayer electrolytes, nanostructures LSM-YDB cathodes and Ni-GDC anodes (LSM-YDB/YDB/YSZ/Ni-GDC). Figure 7.10a shows the temperature dependence of the electrochemical performance of the fabricated YDB/YSZ supported SOFCs at the temperature range 500 – 600 °C. The open circuit voltage (OCV) value was 0.64 V at 600 °C and had a slightly decreasing trend with increasing temperature, as expected. The peak power density was determined as 0.02 W/cm² at 600 °C. This value is rather lower than what can be expected from a fuel cell with this configuration. To determine the reasons for the relatively low power density, electrochemical impedance spectroscopy was performed on the fuel cells. From, the Nyquist graph, it can be determined that the cell had ohmic and electrode polarization resistances of ca. 2.8 and 3.5 Ωcm² at 600 °C,

respectively. The ohmic resistance obtained in the fuel cell is consistent with what was obtained in the conductivity measurements, which is much higher than expected from the given YSZ/YDB bilayer electrolyte configuration. This has been linked to the lack of crystallinity of the deposited YSZ layer. Furthermore, the electrode polarization resistance of 3.5 $\Omega.cm^2$ is larger than the total of what was reported for the polymeric precursor derived Ni-GDC and LSM-YDB electrodes (0.50 and 0.55 $\Omega.cm^2$, respectively). Although the optimization of the electrode deposition conditions is beyond the scope of this work, it is expected that the electrode performances obtained in previous works can be realized in the present fuel cell configuration.

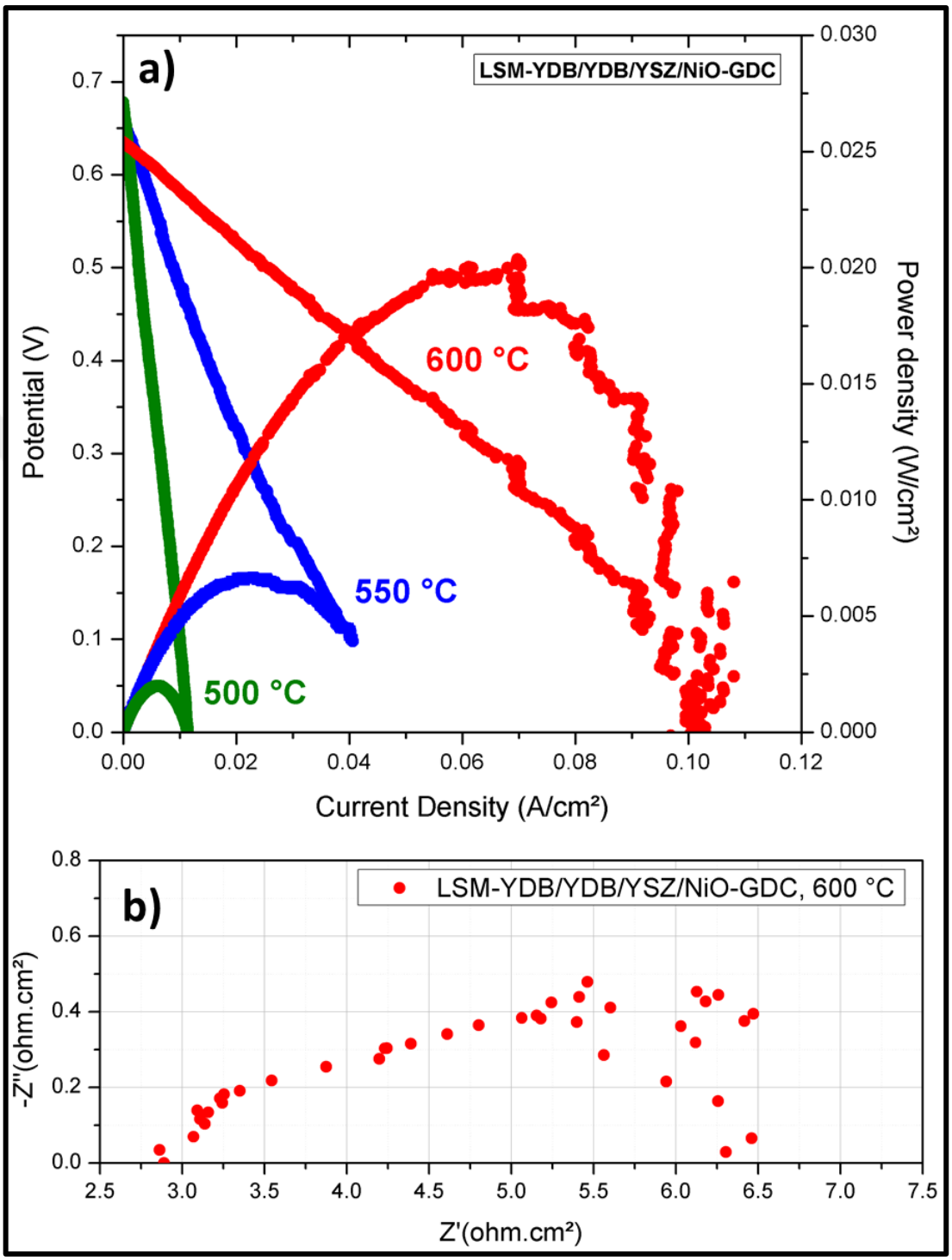

Figure 7. 10: a) The I-V and I-P characteristic of YDB/YSZ full cell at temperature range of 500 - 600 °C and b) Nyquist graph of YSZ/YDB full cell at 600 °C

8. CONCLUSION

Immense ionic conductivity of yttria doped bismuth oxide (YDB) is known and that makes it a promising candidate for intermediate temperature SOFCs. However, YDB reduces to metallic Bi when it contacts with fuel at the targeted operating temperatures. For this purpose, we have developed a bilayer electrolyte consisting of a ca. 200 µm – thick YDB and a 500 nm-thick YSZ layer to set the stage for the fabrication of electrolyte supported SOFCs. It was envisioned that, the tape-cast YDB would act as the main electrolyte and mechanical support, while the polymeric precursor-derived, thin YSZ would prevent the reduction of YDB under anode conditions.

Since for this vision to be realized, the applied YSZ coating must be extremely thin and crack-free, our efforts focused on the optimization of the YSZ deposition parameters to ensure homogeneous and crack-free film formation on YDB substrates. To investigate the effectiveness of YSZ layers, microstructural investigations were performed by scanning electron microscopy and electrochemical measurements were taken using a potentiostat in different ambiances. Our experiments showed that the generic Zr source used in the polymeric precursor derived method, zirconium oxychloride octahydrate, does not effectively complete polymerization, which, in turn, led to crack formation in thin films. To overcome that issue, the addition of nitric acid was supposed to eliminate cracks are in thin films due to the catalyzation of ethylene glycol appropriately. However, thin films derived from a polymeric precursor with nitric acid form cracks when they were exposed to heat treatment at 600 °C. The observed cracks after heat treatment were associated with bismuth yttrium oxychloride these results corresponded to our XRD and SEM-EDX results. On the other hand, switching from the generic Zr source to zirconium oxynitrate hydrate resulted in a completely polymerized solution as it released nitric acid into the solution. Additionally, the absence of the Cl anion in the polymeric precursor prevented the formation of bismuth yttrium oxychloride led to crack-free and dense YSZ coating even after heat treatment at 600 °C. Electrical conductivities of thin films obtained from different polymeric precursors are somewhat lower than the crystalline YSZ because of their poorly crystallized nature.

Optimized crack-free and dense thin films were investigated under fuel flow and we obtained promising results that the bismuth oxide was not reduced to Bi metal for 26 h.

Fuel cells with the developed bilayer electrolyte and polymeric precursor-derived nanocomposite electrodes were constructed. The performance measurements revealed lower power densities than expected, likely due to i) the extra resistance caused by the amorphous nature of the applied YSZ coating and ii) non-optimized electrode fabrication conditions.

REFERENCES

[1] IEA, (2015), "World energy outlook 2015".

[2] Seh Z. W., Kibsgaard J., Dickens C. F., Chorkendorff I., Nørskov J. K., Jaramillo T. F., (2017), "Combining theory and experiment in electrocatalysis: Insights into materials design", Science, 355 (6321).

[3] Web 1, https://www.energy.gov/eere/fuelcells/comparison-fuel-cell-technologies, (Accessed Date: 26/12/2020).

[4] Barbir F., (2005), "Pem fuel cells : Theory and practice", 2nd Edition, Elsevier Academic.

[5] Wachsman E. D., Lee K. T., (2011), "Lowering the temperature of solid oxide fuel cells", Science, 334 (6058), 935-939.

[6] Singhal S. C., Kendall K., "High-temperature solid oxide fuel cells : Fundamentals, design, and applicatons" Elsevier Science Ltd, 1st Edition, Oxford, UK.

[7] Gao Z., Mogni L. V., Miller E. C., Railsback J. G., Barnett S. A., (2016), "A perspective on low-temperature solid oxide fuel cells", Energy & Environmental Science, 9 (5), 1602-1644.

[8] Faes A., Hessler-Wyser A., Zryd A., Van herle J., (2012), "A review of redox cycling of solid oxide fuel cells anode", Membranes, 2 (3), 585-664.

[9] Hayashi H., (2000), "Thermal expansion of gd-doped ceria and reduced ceria", Solid State Ionics, 132 (3-4), 227-233.

[10] Kharton V. V., Figueiredo F. M., Navarro L., Naumovich E. N., Kovalevsky A. V., Yaremchenko A. A., Viskup A. P., Carneiro A., Marques F. M. B., Frade J. R., (2001), Journal of Materials Science, 36 (5), 1105-1117.

[11] Huang H., Gür T. M., Saito Y., Prinz F., (2006), "High ionic conductivity in ultrathin nanocrystalline gadolinia-doped ceria films", Applied Physics Letters, 89 (14), .

[12] Jiang N., Wachsman E. D., (2004), "Structural stability and conductivity of phase-stabilized cubic bismuth oxides", Journal of the American Ceramic Society, 82 (11), 3057-3064.

[13] Boyapati S., Wachsman E., Jiang N., (2001), "Effect of oxygen sublattice ordering on interstitial transport mechanism and conductivity activation energies in phase-stabilized cubic bismuth oxides", Solid State Ionics, 140 (1-2), 149-160.

[14] Yun B.-H., Lee C.-W., Jeong I., Lee K. T., (2017), "Dramatic enhancement of long-term stability of erbia-stabilized bismuth oxides via quadrivalent hf doping", Chemistry of Materials, 29 (24), 10289-10293.

[15] Fung K. Z., Chen J., Virkar A. V., (1993), "Effect of aliovalent dopants on the kinetics of phase transformation and ordering in re2o3-bi2o3 (re = yb, er, y, or dy) solid solutions", Journal of the American Ceramic Society, 76 (10), 2403-2418.

[16] Fung K., Baek H., Virkar A., (1992), "Thermodynamic and kinetic considerations for bi2o3-based electrolytes", Solid State Ionics, 52 (1-3), 199-211.

[17] Kruidhof H., (1990), "Thermochemical stability and nonstoichiometry of yttria-stabilized bismuth oxide solid solutions", Solid State Ionics, 37 (2-3), 213-215.

[18] Takahashi T., Esaka T., Iwahara H., (1975), "High oxide ion conduction in the sintered oxides of the system bi2o3-gd2o3", Journal of Applied Electrochemistry, 5 (3), 197-202.

[19] Kruidhof H., Bouwmeester H., Devries K., Gellings P., Burggraaf A., (1992), "Thermochemical stability and nonstoichiometry of erbia-stabilized bismuth oxide", Solid State Ionics, 50 (1-2), 181-186.

[20] Jiang S. P., (2003), "Sintering behavior of ni/y2o3-zro2cermet electrodes of solid oxide fuel cells", Journal of Materials Science, 38 (18), 3775-3782.

[21] Simwonis D., (2000), "Nickel coarsening in annealed ni/8ysz anode substrates for solid oxide fuel cells", Solid State Ionics, 132 (3-4), 241-251.

[22] Liu Y. L., Thydén K., Chen M., Hagen A., (2012), "Microstructure degradation of lsm-ysz cathode in sofcs operated at various conditions", Solid State Ionics, 206 97-103.

[23] Jørgensen M. J., Holtappels P., Appel C. C., (2000), Journal of Applied Electrochemistry, 30 (4), 411-418.

[24] Jiang S. P., (2008), "Development of lanthanum strontium manganite perovskite cathode materials of solid oxide fuel cells: A review", Journal of Materials Science, 43 (21), 6799-6833.

[25] Hardy J. S., Templeton J. W., Edwards D. J., Lu Z., Stevenson J. W., (2012), "Lattice expansion of lscf-6428 cathodes measured by in situ xrd during sofc operation", Journal of Power Sources, 198 76-82.

[26] Jung W., Tuller H. L., (2012), "Investigation of surface sr segregation in model thin film solid oxidefuel cell perovskite electrodes", Energy Environ. Sci., 5 (1), 5370-5378.

[27] Koo B., Kim K., Kim J. K., Kwon H., Han J. W., Jung W., (2018), "Sr segregation in perovskite oxides: Why it happens and how it exists", Joule, 2 (8), 1476-1499.

[28] Lee W., Han J. W., Chen Y., Cai Z., Yildiz B., (2013), "Cation size mismatch and charge interactions drive dopant segregation at the surfaces of manganite perovskites", Journal of the American Chemical Society, 135 (21), 7909-7925.

[29] Kim S., Moon H., Hyun S., Moon J., Kim J., Lee H., (2006), "Performance and durability of ni-coated ysz anodes for intermediate temperature solid oxide fuel cells", Solid State Ionics, 177 (9-10), 931-938.

[30] Buyukaksoy A., Petrovsky V., Dogan F., (2011), "Redox stable solid oxide fuel cells with ni-ysz cermet anodes prepared by polymeric precursor infiltration", Journal of The Electrochemical Society, 159 (2), B232-B234.

[31] Buyukaksoy A., Petrovsky V., Dogan F., (2012), "Optimization of redox stable ni-ysz anodes for sofcs by two-step infiltration", Journal of The Electrochemical Society, 159 (12), F841-F848.

[32] Gannon P., Amendola R., (2012), "High-temperature, dual-atmosphere corrosion of solid-oxide fuel cell interconnects", Jom, 64 (12), 1470-1476.

[33] Steele B., (1998), "Properties of la0.6sr0.4co0.2fe0.8o3−x (lscf) double layer cathodes on gadolinium-doped cerium oxide (cgo) electrolytes ii. Role of oxygen exchange and diffusion", Solid State Ionics, 106 (3-4), 255-261.

[34] Eksioglu A., Colakerol Arslan L., Sezen M., Ow-Yang C., Buyukaksoy A., (2019), "Formation of nanocomposite solid oxide fuel cell cathodes by preferential clustering of cations from a single polymeric precursor", ACS Applied Materials & Interfaces, 11 (51), 47904-47916.

[35] Østergård M. J. L., Clausen C., Bagger C., Mogensen M., (1995), "Manganite-zirconia composite cathodes for sofc: Influence of structure and composition", Electrochimica Acta, 40 (12), 1971-1981.

[36] Murata K., Fukui T., Abe H., Naito M., Nogi K., (2005), "Morphology control of la(sr)fe(co)o3−a cathodes for it-sofcs", Journal of Power Sources, 145 (2), 257-261.

[37] Harboe S., Lupetin P., Guillon O., Menzler N. H., (2020), "Investigation of lsm/8ysz cathode within an all-ceramic sofc, part ii: Optimization of performance and co-sinterability", Journal of the European Ceramic Society, 40 (10), 3618-3631.

[38] Fan X., You C.-Y., Zhu J.-L., Chen L., Xia C.-R., (2015), "Fabrication of lsm-sdc composite cathodes for intermediate-temperature solid oxide fuel cells", Ionics, 21 (8), 2253-2258.

[39] Cheng Y., Yu A. S., Li X., Oh T.-S., Vohs J. M., Gorte R. J., (2015), "Preparation of sofc cathodes by infiltration into lsf-ysz composite scaffolds", Journal of The Electrochemical Society, 163 (2), F54-F58.

[40] Klemensø T., Thydén K., Chen M., Wang H.-J., (2010), "Stability of ni–yttria stabilized zirconia anodes based on ni-impregnation", Journal of Power Sources, 195 (21), 7295-7301.

[41] Huang Y.-L., Hussain A. M., Wachsman E. D., (2018), "Nanoscale cathode modification for high performance and stable low-temperature solid oxide fuel cells (sofcs)", Nano Energy, 49 186-192.

[42] Jiang S. P., (2012), "Nanoscale and nano-structured electrodes of solid oxide fuel cells by infiltration: Advances and challenges", International Journal of Hydrogen Energy, 37 (1), 449-470.

[43] Bilbey B., (2020), "Powder and thin film based ni-ysz anodes fabricated from polymeric precursors for solid oxide fuel cells", Yüksek Lisans Tezi, Gebze Technical University.

[44] Zeng Y., Lin Y. S., (1999), "Stability and surface catalytic properties of fluorite-structured yttria-doped bismuth oxide under reducing environment", Journal of Catalysis, 182 (1), 30-36.

[45] Wachsman E., Ball G., Jiang N., Stevenson D., (1992), "Structural and defect studies in solid oxide electrolytes", Solid State Ionics, 52 (1-3), 213-218.

[46] Sammes N. M., Tompsett G. A., Näfe H., Aldinger F., (1999), "Bismuth based oxide electrolytes— structure and ionic conductivity", Journal of the European Ceramic Society, 19 (10), 1801-1826.

[47] Dordor P., (1987), "Electrical characterization of phase transition in yttrium doped bismuth oxide, bi1.55y0.45o3", Solid State Ionics, 25 (2-3), 177-181.

[48] Ayhan Y. S., Buyukaksoy A., (2019), "Impact of fabrication temperature on the stability of yttria doped bismuth oxide ceramics", Solid State Ionics, 338 66-73.

[49] Jung D. W., Lee K. T., Wachsman E. D., (2016), "Dysprosium and gadolinium double doped bismuth oxide electrolytes for low temperature solid oxide fuel cells", Journal of The Electrochemical Society, 163 (5), F411-F415.

[50] Jung D. W., Nino J. C., Duncan K. L., Bishop S. R., Wachsman E. D., (2010), "Enhanced long-term stability of bismuth oxide-based electrolytes for operation at 500 °c", Ionics, 16 (2), 97-103.

[51] Fung K. Z., Virkar A. V., (1991), "Phase stability, phase transformation kinetics, and conductivity of y2o3-bi2o3 solid electrolytes containing aliovalent dopants", Journal of the American Ceramic Society, 74 (8), 1970-1980.

[52] Park J.-Y., Yoon H., Wachsman E. D., (2005), "Fabrication and characterization of high-conductivity bilayer electrolytes for intermediate-temperature solid oxide fuel cells", Journal of the American Ceramic Society, 88 (9), 2402-2408.

[53] Joh D. W., Park J. H., Kim D., Wachsman E. D., Lee K. T., (2017), "Functionally graded bismuth oxide/zirconia bilayer electrolytes for high-performance intermediate-temperature solid oxide fuel cells (it-sofcs)", ACS Applied Materials & Interfaces, 9 (10), 8443-8449.

[54] Virkar A. V., (2019), "Theoretical analysis of solid oxide fuel cells with two-layer, composite electrolytes: Electrolyte stability", Journal of The Electrochemical Society, 138 (5), 1481-1487.

[55] Chan S., Chen J., A. K., (2003), "A simple bilayer electrolyte model for solid oxide fuel cells", Solid State Ionics, 158 (1-2), 29-43.

[56] de Souza S., (1997), "Thin-film solid oxide fuel cell with high performance at low-temperature", Solid State Ionics, 98 (1-2), 57-61.

[57] Ahn J. S., Camaratta M. A., Pergolesi D., Lee K. T., Yoon H., Lee B. W., Jung D. W., Traversa E., Wachsman E. D., (2010), "Development of high performance ceria/bismuth oxide bilayered electrolyte sofcs for lower temperature operation", Journal of The Electrochemical Society, 157 (3).

[58] Lee K. T., Jung D. W., Camaratta M. A., Yoon H. S., Ahn J. S., Wachsman E. D., (2012), "Gd0.1ce0.9o1.95/er0.4bi1.6o3 bilayered electrolytes fabricated by a simple colloidal route using nano-sized er0.4bi1.6o3 powders for high performance low temperature solid oxide fuel cells", Journal of Power Sources, 205 122-128.

[59] Gao Z., Zenou V. Y., Kennouche D., Marks L., Barnett S. A., (2015), "Solid oxide cells with zirconia/ceria bi-layer electrolytes fabricated by reduced temperature firing", Journal of Materials Chemistry A, 3 (18), 9955-9964.

[60] Kim J., Kim J., Yoon K. J., Son J.-W., Lee J.-H., Lee J.-H., Lee H.-W., Ji H.-I., (2020), "Solid oxide fuel cells with zirconia/ceria bilayer electrolytes via roll calendering process", Journal of Alloys and Compounds, 846.

[61] Pesaran A., Jaiswal A., Wachsman E. D., Chapter 1. Bilayer electrolytes for low temperature and intermediate temperature solid oxide fuel cells – a review, in Energy storage and conversion materials. 2019. p. 1-41.

[62] Wachsman E., (2002), "Functionally gradient bilayer oxide membranes and electrolytes", Solid State Ionics, 152-153 657-662.

[63] Wachsman E. D., Jayaweera P., Jiang N., Lowe D. M., Pound B. G., (1997), "Stable high conductivity ceria/bismuth oxide bilayered electrolytes", Journal of The Electrochemical Society, 144 (1), 233-236.

[64] Holzer L., Iwanschitz B., Hocker T., Münch B., Prestat M., Wiedenmann D., Vogt U., Holtappels P., Sfeir J., Mai A., Graule T., (2011), "Microstructure degradation of cermet anodes for solid oxide fuel cells: Quantification of nickel grain growth in dry and in humid atmospheres", Journal of Power Sources, 196 (3), 1279-1294.

[65] Anderson H. U., Nasrallah M. M., Chen C. C., (1996), "Method of coating a substrate with a metal oxide film from an aqueous solution comprising a metal cation and a polymerizable organic solvent", U.S. Patent, 494-700.

[66] Buyukaksoy A., Petrovsky V., Dogan F., (2013), "Solid oxide fuel cells with symmetrical pt-ysz electrodes prepared by ysz infiltration", Journal of The Electrochemical Society, 160 (4), F482-F486.

[67] Demirkal E., Büyükaksoy A., (2019), "Gümüş akim toplayici mürekkeplerİnde frİt bulunmasinin kati oksİt yakit hücresİ katotlarinin elektrokİmyasal performansina etkİsİ", Mühendislik Bilimleri ve Tasarım Dergisi, 7 (4), 796-802.

[68] Aktaş B., (2019), "Düşük sıcaklıkta çalışan katı oksit yakıt hücreleri için bi2o3 temelli kompozit ince film katotların geliştirilmesi", Yüksek Lisans Tezi, Gebze Technical University.

[69] Wu Y.-C., Chang Y.-W., Wang S.-F., (2013), "Electrical properties and microstructural analysis of aliovalent-ion (y3+, nb5+)–doped bismuth-based solid-oxide electrolyte", Ferroelectrics, 455 (1), 123-128.

[70] Hayashi H., Saitou T., Maruyama N., Inaba H., Kawamura K., Mori M., (2005), "Thermal expansion coefficient of yttria stabilized zirconia for various yttria contents", Solid State Ionics, 176 (5-6), 613-619.

[71] Chen C. C., Nasrallah M. M., Anderson H. U., (2019), "Synthesis and characterization of (ceo2) 0.8 (smo1.5) 0.2 thin films from polymeric precursors", Journal of The Electrochemical Society, 140 (12), 3555-3560.

[72] Liu Z., Li J., Ya J., Xin Y., Jin Z., (2008), "Mechanism and characteristics of porous zno films by sol–gel method with peg template", Materials Letters, 62 (8-9), 1190-1193.

[73] Huang W., Lei M., Huang H., Chen J., Chen H., (2010), "Effect of polyethylene glycol on hydrophilic tio2 films: Porosity-driven superhydrophilicity", Surface and Coatings Technology, 204 (24), 3954-3961.

[74] Petrovsky V., Suzuki T., Jasinski P., Petrovsky T., Anderson H. U., (2004), "Low-temperature processing of thin-film electrolyte for electrochemical devices", Electrochemical and Solid-State Letters, 7 (6).

[75] Park J.-Y., Wachsman E. D., (2006), "Stable and high conductivity ceria/bismuth oxide bilayer electrolytes for lower temperature solid oxide fuel cells", Ionics, 12 (1), 15-20.

[76] Buyukaksoy A., Kammampata S. P., Birss V. I., (2015), "Effect of porous ysz scaffold microstructure on the long-term performance of infiltrated ni-ysz anodes", Journal of Power Sources, 287 349-358.

APPENDICES

Appendix A: Publications Made Within the Scope of the Thesis

Bal B., Buyukaksoy A., "Effect of precursor solution parameters on the formation of yttria stabilized zirconia coatings on yttria stabilized bismuth oxide substrates", International Journal of Hydrogen Energy, 2020, DOI: 10.1016/j.ijhydene.2020.09.223.

Bal B., Buyukaksoy A., "Fabrication of Dense Yttria Stabilized Zirconia Coatings and Their Evaluation as a Solid Oxide Fuel Cell Electrolyte", 4th International Symposium on Materials for Energy Storage and Conversion (^{m}ESC-IS), 11-13 September 2019, Akyaka, Mugla, Turkey.

Appendix B: Fabrication of Dense Yttria Stabilized Zirconia Coatings Using Powder Containing Polymeric Precursor

Production of thin-film electrolytes for low-temperature fuel cell applications using polymeric precursor-based methods has been reported by several studies [34, 43, 68, 74]. Low fabrication temperatures of thin-film electrolytes (under 1000 °C) can prevent possible undesired reactions at the electrolyte/cathode interface, which has been a significant problem [7]. The experiments reported in this study up to this point have reported the use of polymeric precursors to fabricate crack-free YSZ coatings with thicknesses of several hundred nanometers. However, especially in the case of YDB, thicker crack-free YSZ coatings may be required to obtain even higher open circuit potentials. But, increasing the film thickness is problematic since it brings about the possibility of crack formation due to larger stresses. To reduce these stresses, Petrovksy et al proposed to first to form a porous YSZ scaffold on the substrate by depositing a suspension containing the YSZ powders and then to infiltrate this porous scaffold with polymeric YSZ precursor to densify it. [74]. Here, we have attempted to use a single suspension prepared by mixing YSZ powder with polymeric YSZ precursor. This way, we aimed at reducing the film shrinkage and thus, avoiding crack formation.

- Preparation and Deposition of Powder Containing YSZ Polymeric Precursor

An 8% mol Y_2O_3 stabilized ZrO_2 (YSZ) polymeric precursor was prepared using the proper amounts of yttrium (III) nitrate hexahydrate (Alfa Aesar, 99.8% trace metal basis) and zirconium oxychloride octahydrate (Sigma Aldrich, 98% reagent grade). After the nitrate salts were dissolved in de-ionized water, ethylene glycol was added into the obtained clear solution and heated up to 120 °C while the solution was stirring until polymerization was completed. Ethanol and YSZ powder mixture (Tosoh Corp., 8 mol % yttria) was prepared in an ethanol to YSZ powder weight ratio of 75:6.5 and milled in a PTFE bottle with 100 gr ZrO_2 milling media for 24 hours to obtain a homogenous and well-dispersed suspension. After obtaining a YSZ powder containing slurry and completely polymerized YSZ polymeric precursor, three types of powder-containing-polymeric precursor with different YSZ powder to YSZ polymeric precursor weight ratios (1:1, 1:5, and 1:11) were prepared. Then the prepared suspensions were stirred on

a hot plate at room temperature until the ethanol into the suspension evaporated and then, 2-butoxyethanol was added to stabilize the surface energy of the suspension and to improve its wetting ability.

For deposition, a dip-coater was used with different withdrawal rates and different deposition cycles. Microscope slides and YDB-1100 ceramics were used as a substrate for deposition. After each deposition cycle, deposited substrates were heated up on a hot plate using a ramping rate of 12.5 °C per minute from room temperature to 350 °C, then, the hot plate was turned off and samples remained on it until they cooled down. YDB-1100 ceramics allowed us to investigate the sinterability of YSZ coatings at relatively low temperatures. After determining the optimum deposition parameters of YSZ coatings, the films fabricated on YDB-1100 ceramics and heat-treated at 1100 °C to investigate the sinterability of the films.

- Characterization of Prepared Solutions and YSZ Coatings

After the addition of 2-butoxyetanol, to obtain a well-dispersed suspension, the surface polarization of commercially available YSZ powders in suspension was investigated by zeta-potential measurements using Zetasizer Nano-ZS. For surface electrical potential measurements two suspensions were selected (1:1 and 1:11) to understand boundary conditions. A typical zeta-potential measurement was applied using HCl and KOH to tune the pH values within the 1 – 12 range.

Microstructural characterization of deposited thin films was performed by scanning electron microscopy (SEM – Philips XL 30 S FEG) using its secondary electron microscopy mode to investigate the crack formation of the thin films as-deposited/dried state and after heat treatment at 1100 °C for 2 h.

- Results and Discussion

Figure B.1 shows the top-surface SEM images of the YSZ coatings deposited onto glass substrates using suspensions containing YSZ powders and polymeric precursors in 1:11, 1:5 and 1:1 weight ratios. Evidently, the coating deposited from the suspension containing the smallest amount of YSZ had crack-free surfaces (powder to polymeric precursor weight ratio of 1:11) (Figure B.1 a and b). Meanwhile, increasing the powder

content in the suspensions resulted in the formation of larger clusters and cracks in their vicinity (Figure B.1 c-f).

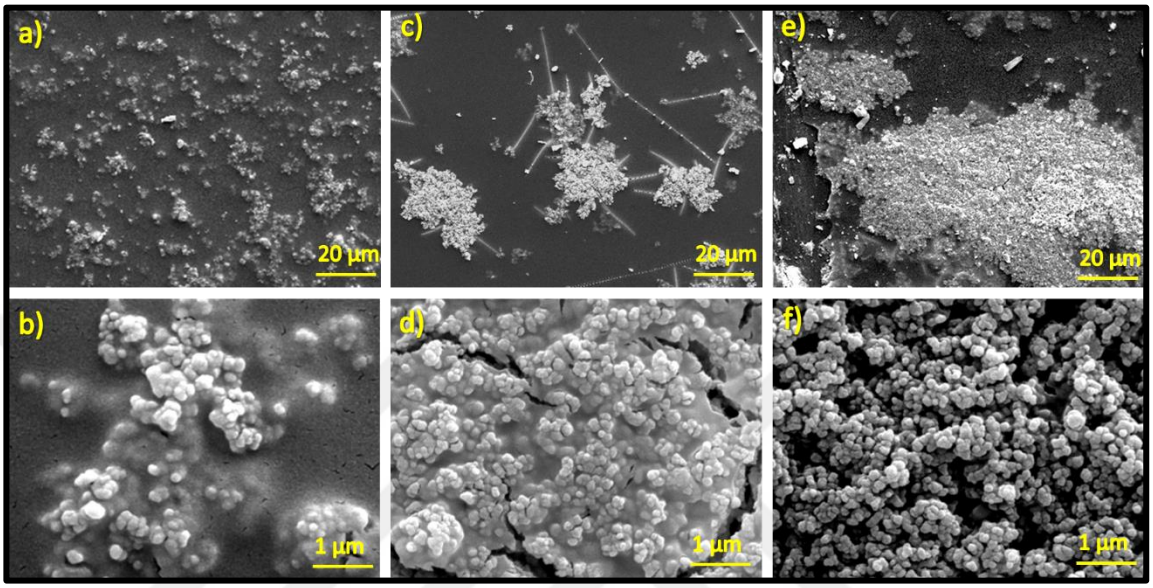

Figure B1.1: Top surface SEM images of powder-containing-YSZ polymeric precursor derived YSZ coatings with different polymeric precursor to YSZ powder a) 1 to 11 and b) higher magnification, c) 1 to 5 and d) higher magnification, e) 1 to 1 f) higher magnifications.

To optimize the deposition conditions, we have also varied the withdrawal rates used during the dip-coating process, while keeping the powder to polymeric precursor ratio constant at 1 : 11 (Figure B.2). The presence of the amorphous phase increased as the withdrawal rate increased. It can be suggested that slow withdrawal rates allow more polymeric precursor to be poured back into the beaker, hence leaving a larger amount of powder behind. At very fast withdrawal rates of 200 mm/min, cracks within the amorphous phase is observed, while in much slower withdrawal rates, mud cracks within the powder clusters are observed (Figure B.2a and b). The case in which withdrawal rate of 100 mm/min was used produces crack-free coatings (Figure B.3c and d).

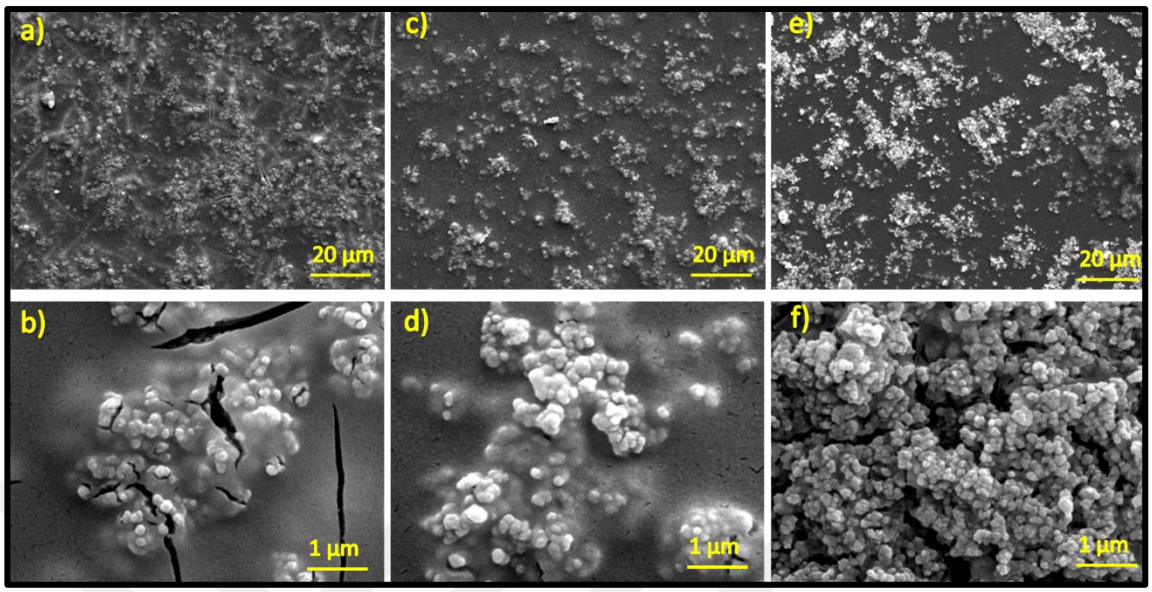

Figure B1.2: Crack formation with respect to withdrawal rate a) 200 mm/min and b) higher magnification, c) 100 mm/min and d) higher magnification, e) 50 mm/min and f) higher modification for weight ratio of 1 to 11 coatings.

For further optimization, we have varied the number of deposition/drying cycles, while keeping the withdrawal rate and powder to polymeric precursor weight ratio (Figure B.3). Increasing the thickness by increasing the number of depositions resulted in crack formation, suggesting that 5 depositions of the suspension with the 1:11 solids loading performed at 100 mm/min is the optimum deposition condition for crack free YSZ coatings.

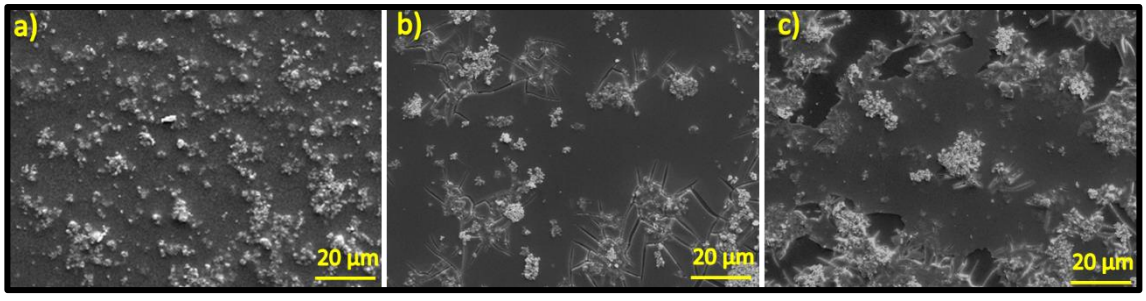

Figure B1.3: Crack formation with respect to deposition cycle a) 5 times, b) 10 times and c) 15 times deposited powder-containing-YSZ polymeric precursor.

In our experiments on glass substrates, the common observation was that the YSZ powders tend to form clusters. To determine the conditions in which these clusters

would not form, we have measured zeta potentials with under different pH conditions. Figure B.4 shows the zeta potentials of suspensions with 1 : 1 and 1 : 11 powder to polymeric precursor ratios. In both cases, suspensions appear to be stable at pH values lower that 4 and higher than 10.

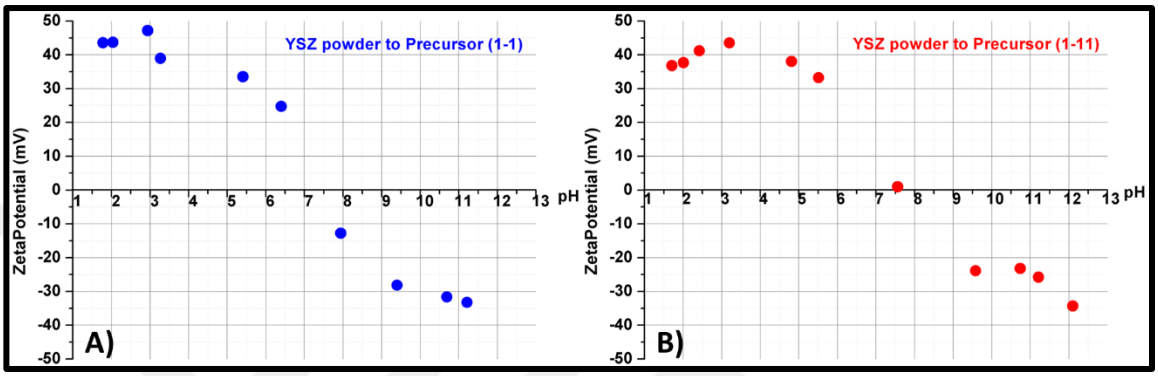

Figure B1.4: Zeta-potential values of powder-containing-YSZ polymeric precursor with powder to polymeric precursor ratio a) 1 to 1 and b) 1 to 11.

The microscope slides have not allowed heat treatment due to their low melting temperature. Therefore, YDB-1100 ceramics were used as a substrate to test the sinterability of optimum coatings. Powder-containing-YSZ polymeric precursors (powder to polymeric precursor ratio of 1:1) were deposited onto YDB-1100 ceramics for 15 cycles using a rpm of 1500 and heat treated at 1100 °C for 2 h. Highly dense YSZ layers were obtained after heat treatment (Figure B.5). Considering that prepared previous study by Buyukaksoy et al. reported that a YSZ suspension sintered at 1150 °C for 2 h resulted in a 49% open porosity[76], it can be suggested that the powder-polymeric precursor mixture in fact, worked fine to reduce the sintering temperature. However, in lower magnification images (not shown here) large cracks, which would allow hydrogen – bismuth oxide contact, were present at the coating surface.

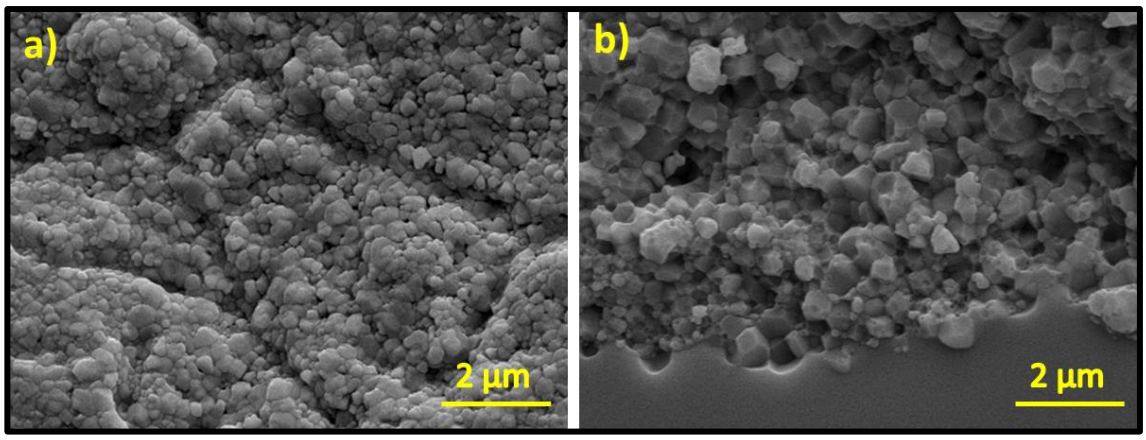

Figure B1.5: a) Top surface and b) interface between fired YSZ coating at 1100 °C for 2h and YDB-1100.

- Summary

In this part of the study, the development of yttria-stabilized zirconia coatings on dense yttria-doped bismuth oxide (YDB) ceramics using a mixture of commercially available YSZ powders and YSZ polymeric precursor was presented. This way thicker YSZ coatings than those derived polymeric precursors were aimed. Optimum powder to polymeric precursor ratios and dip-coating parameters (withdrawal speed, number of deposition layers etc.) were determined to ensure crack-free coatings on glass substrates. On YDB substrates, although thick, dense YSZ coatings were achieved after sintering only at 1150 °C, crack formation could not be avoided.